Biomaterials 269 (2021) 120633

Contents lists available at ScienceDirect

Biomaterials

journal homepage: www.elsevier.com/locate/biomaterials

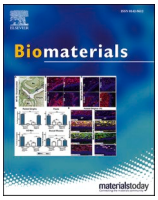

Dissecting the effects of preconditioning with inflammatory cytokines and hypoxia on the angiogenic potential of mesenchymal stromal cell (MSC)-derived soluble proteins and extracellular vesicles (EVs)

Cansu Gorgun [a,b], Davide Ceresa [b], Raphaelle Lesage [c,d], Federico Villa [b], Daniele Reverberi [e], Carolina Balbi [f], Sara Santamaria [a], Katia Cortese [a], Paolo Malatesta [a,b], Liesbet Geris [c,d,g], Rodolfo Quarto [a,b], Roberta Tasso [a,b,*]

[a] Department of Experimental Medicine (DIMES), University of Genova, Genova, Italy
[b] U.O. Cellular Oncology, IRCCS Ospedale Policlinico San Martino, Genova, Italy
[c] Prometheus, Division of Skeletal Tissue Engineering, KU Leuven, Leuven, Belgium
[d] Biomechanics Section, Department of Mechanical Engineering, KU Leuven, Leuven, Belgium
[e] U.O. Molecular Pathology, IRCCS Ospedale Policlinico, San Martino, Genova, Italy
[f] Laboratory of Cellular and Molecular Cardiology, Cardiocentro Ticino Foundation, 6900, Lugano, Switzerland
[g] Biomechanics Research Unit, GIGA in Silico Medicine, University of Liège, Liège, Belgium

ARTICLE INFO

Keywords:
Mesenchymal stromal cells
Extracellular vesicles
Angiogenesis
RNASeq
Proteomics
Regenerative medicine

ABSTRACT

Mesenchymal stromal cells (MSCs) are characterized by a regulatory phenotype and respond promptly to the environmental signals modulating their secretory activity. An appropriate preconditioning may induce MSCs to release secretomes with an enhanced regenerative potential. However, it fails to take into account that secretomes are composed by both soluble factors and extracellular vesicles (EVs), whose functions could be altered differently by the preconditioning approach. Here we demonstrate that the MSC secretome is strongly modulated by the simultaneous stimulation with hypoxia and pro-inflammatory cytokines, used to mimic the harsh environment present at the site of injury. We observed that the environmental variations strongly influenced the angiogenic potential of the different secretome fractions. Upon inflammation, the pro-angiogenic capacity of the soluble component of the MSC secretome was strongly inhibited, regardless of the oxygen level, while the EV-encapsulated component was not significantly affected by the inflammatory stimuli. These effects were accompanied by the modulation of the secreted proteins. On one hand, inflammation-activated MSCs release proteins mainly involved in the interaction with innate immune cells and in tissue remodeling/repair; on the other hand, when MSCs are not exposed to an inflamed environment, they respond to the different oxygen levels modulating the expression of proteins involved in the angiogenic process. The cargo content (in terms of miRNAs) of the corresponding EV fractions was less sensitive to the influence of the external stimuli. Our findings suggest that the therapeutic efficacy of MSC-based therapies could be enhanced by selecting the appropriate preconditioning approach and carefully discriminating its effects on the different secretome components.

1. Introduction

Mesenchymal Stromal Cells (MSCs) are versatile progenitors able to sense the surrounding environment and actively respond to changes or requirements of the milieu modulating the secretion of specific mediators [1]. It's widely accepted that in many experimental and clinical settings the MSC potency and therapeutic efficacy do not depend on the physical closeness of the transplanted cells to the damaged tissue, but rather on their paracrine activity [2,3]. The array of trophic factors and extracellular vesicles (EVs) secreted by MSCs is broadly defined as the cell secretome. When MSCs are injected *in vivo* and encounter the harsh environment typical of a damaged tissue, they face a decline in their biological performances [4]. Preconditioning represents an adaptive strategy to improve MSC therapeutic efficacy, preparing cells to survive in hostile conditions and enhancing their regulatory activities [5,6]. In this context, one of the major challenges in MSC-based therapies is to

* Corresponding author. Department of Experimental Medicine (DIMES), University of Genova, Genova, Italy.
E-mail address: roberta.tasso@unige.it (R. Tasso).

https://doi.org/10.1016/j.biomaterials.2020.120633
Received 18 August 2020; Received in revised form 30 November 2020; Accepted 22 December 2020
Available online 28 December 2020
0142-9612/

develop *in vitro* culture methods that mimic the injury environment, without compromising cell quality and function. Strong inflammation and hypoxia are two simultaneous and related conditions during the early phases of the tissue healing process [7,8]. Indeed, in the context of the wound microenvironment, the activation of innate immune cells, mainly neutrophils and monocytes, results in an enhanced release of chemokines and cytokines, such as Tumor Necrosis Factor-α (TNF-α) and Interleukin-1α and -1β (IL-1α and IL-1β), that act as mediators of the host defense [9]. In these phases, wound sites are also characterized by low oxygen tension due to disruption of the vasculature surrounding the injury [7]. This is the complex milieu that transplanted MSCs encounter and that mitigate their function and survival; treating cells with the same stimuli before transplantation could overcome these limitations and enhance their paracrine activity [4,10].

The control of blood vessel growth plays a key role to restore blood supply and ensure rapid vascularization of damaged tissues [11]. Several literature reports indicate that MSC secretome can exert different effects in the context of angiogenesis, and many of these differences largely depends upon the various culture conditions [12,13]. It has been described that MSCs respond positively to hypoxic preconditioning, showing a decreased apoptosis even in severe microenvironmental conditions and an increased expression of angiogenic factors [14,15]. Although various cytokines and chemical compounds have been proven to have cell-protective effects [16], contrasting results have been published regarding the angiogenic potential of MSCs licensed by a pro-inflammatory microenvironment [17–19].

In the present study we evaluated the influence of a short-term preconditioning with both hypoxia (1% O_2) and inflammatory stimuli (TNF-α and IL-1α) on the angiogenic potential of human adipose tissue-derived MSC secretome. In particular, we compared the effect of the total conditioned medium (CM) with that exerted by the corresponding fractions composed by either small- or medium-sized extracellular vesicles (sEVs and mEVs), and with the vesicle-depleted medium, enriched only in soluble factors. Extensive *in vitro* and *ex vivo* data demonstrated that the synergistic action of hypoxia and inflammation affected the MSC secretome fractions at different extents. In response to inflammatory cytokines, MSCs released soluble factors with a strong anti-angiogenic effect on endothelial cell proliferation, migration and tubulogenesis. On the contrary, and depending on the specific aspect of the angiogenic process, the corresponding EV fractions were less sensitive to the influence of external stimuli. Our findings suggest that a deep investigation into how preconditioning can specifically influence the different cell paracrine activities is fundamental to provide new insights for the therapeutic use of the MSC secretome.

2. Materials and methods

2.1. Isolation and culture of human adipose tissue-derived Mesenchymal Stromal Cells (MSCs)

MSCs were obtained from subcutaneous adipose tissue, as previously described [20] and in compliance to Regione Liguria Ethical Committee authorization (P.R. 23571). Briefly, subcutaneous adipose tissue in the form of liposuction aspirates was obtained from human healthy donors during routine lipoaspiration after informed consent. Adipose tissue was extensively washed with cold phosphate-buffered saline (PBS) and digested in 0.1% type I Collagenase (Gibco, MI, Italy) in PBS at 37 °C for 60 min. The resulting stromal vascular fraction (SVF) pellet was extensively rinsed and plated at a density equivalent to 2 ml of liposuction tissue aspirate/54cm^2 of surface area and cultured in Dulbecco's MEM (D-MEM) (Biochrom GmbH, Berlin, Germany) supplemented with 10% fetal bovine serum (FBS) (Gibco, Milan, Italy), 2 mM of L-glutamine, and 50 mg/ml penicillin/streptomycin. The cultures were performed in the presence of 1 ng/ml of fibroblast growth factor-2 (FGF-2; Peprotech, Milan, Italy) (standard condition). Medium was changed every 3 days and cells expanded after reaching about 85% confluence using 0.05% trypsin-EDTA (Gibco, MI, Italy). All cultures were maintained in a humidified incubator at 37 °C with 5% CO_2. The immunophenotype was evaluated by flow cytometry on MSC cultured in standard condition using the following monoclonal antibodies to: CD31-FITC (390), CD34-FITC (4H11), CD45-PE (2D1), CD73-FITC (AD2), mouse IgG1 kappa Isotype Control-FITC (P3.6.2.8.1), mouse IgG1 kappa Isotype Control-PE (P3.6.2.8.1) (eBioscience), and monoclonal antibodies to: CD90-PE (5E10), CD29-PE (MAR4), CD105-PE (266), CD44-FITC (L178), mouse IgG1 kappa Isotype Control-FITC (MOPC-21), mouse IgG1 kappa Isotype Control-PE (MOPC-21) (BD Biosciences). Cells were analyzed using a flow cytometer (FACSCanto, BD Biosciences).

The MSC differentiation potential into osteogenic and adipogenic lineages was verified *in vitro*. Briefly, cells cultured in standard condition were detached from cultures reaching 90% confluence, washed, and plated at a concentration of 5x10^4 cells/cm^2 in 24-well culture plates. Osteogenic differentiation was induced by stimulating cultures with 50 mg/ml ascorbic acid, 1.5 mg/ml β-glycerophosphate, and 10^{-7} M dexamethasone in D-MEM for 14 days. The presence of calcium deposits was revealed using Alizarin Red-S staining. To check the adipogenic differentiation potential, MSCs were stimulated for 21 days in D-MEM supplemented with 1% FBS, 10^{-7} M dexamethasone, and 6 ng/ml insulin. Lipid droplets were revealed by staining with Oil Red staining.

Only cells that were in passage 2 or 3 were used for extracellular vesicle separation.

2.2. MSC pre-conditioning and collection of MSC Conditioned Media (CM)

When MSCs reached around 70% confluence, cells were rinsed twice with PBS and maintained for 20 min in D-MEM supplemented with 2 mM L-glutamine and 50 mg/ml penicillin/streptomycin (serum-free medium) to remove FBS residue. Medium was then removed and replaced with fresh serum-free medium and cultures split into four subcultures maintained for 24 h under normoxia (20% O_2) (Nor), hypoxia (1% O_2) (Hyp), normoxia supplemented with 50 ng/ml Tumor Necrosis Factor-α (TNF-α) (PeproTech, London, UK) and 50 ng/ml Interleukin 1-α (IL1-α) (PeproTech, London, UK) (Nor^{INF}), and hypoxia supplemented with 50 ng/ml TNF-α and 50 ng/ml IL1-α (Hyp^{INF}). The immunophenotype of MSCs cultured in Nor, Hyp, Nor^{INF} and Hyp^{INF} conditions was evaluated by flow cytometry exploiting the same anti-human antibodies above described. Cell viability of MSCs cultured for 24 h in Nor, Hyp, Nor^{INF} and Hyp^{INF} conditions was detected by FITC Annexin V Apoptosis Detection Kit (BD Biosciences), according to manufacturer's instructions. Cells were analyzed using a flow cytometer (FACSCanto; BD Biosciences). Conditioned media (CM) from Nor, Hyp, Nor^{INF} and Hyp^{INF} were collected. Half of each CM preparation was used to isolate extracellular vesicles and generate the corresponding amount of depleted medium, as described in the next paragraph, and the other half of CM was concentrated with Amicon®-Ultra-15, 3 kDa centrifugal filter tubes (Merck, Massachusetts, USA). In order to quantify the protein amount, BCA (BicinChoninic Acid) Protein Assay Kit (Thermo Fisher Scientific, Massachusetts, USA) was used.

2.3. Extracellular vesicle (EV) separation and generation of depleted-medium (DM)

We have submitted all relevant data of our experiments to the EV-TRACK knowledgebase (EV-TRACK ID: EV200171) [21]. EVs were separated from Nor-, Hyp-, Nor^{INF}-, and Hyp^{INF}- CM by differential ultracentrifugation using a Beckman Coulter ultracentrifuge (Optima L-90K), according to an already published protocol [22]. After collecting the CM, cells/cell debris and apoptotic bodies were removed centrifuging the CM for 10 min at 300 x*g* and for 20 min at 2000 x*g*, respectively. The resulting supernatant was transferred into ultracentrifugation tubes (Beckman-Coulter, USA) and subjected to a first centrifugation for 40 min at 10.000 x*g* (10K pellet) to obtain an EV

pellet (10K pellet) enriched with medium sized-vesicles (mEVs). Supernatants were then centrifuged for 120 min at 100.000 xg in order to obtain a pellet (100K pellet) enriched with small sized-vesicles (sEVs). Supernatants derived from 100K centrifugation were collected as depleted media (DM) and concentrated to reach the same volume of their corresponding CM. All EV pellets were washed in PBS and centrifuged at the same speed before being resuspended in sterile filtered (0.22 μm) PBS or serum-free medium, in the same volume of their corresponding CM and DM. A SW28 swinging bucket rotor (Beckman Coulter) has been used during the ultracentrifugation steps.

2.4. Flow cytometry characterization of EVs

EV characterization by flow cytometry was performed as previously described [23]. Briefly, each EV preparation was suspended in filtered PBS and distributed in flow cytometry tubes (100 μl/tube). For each preparation, one tube has been stained with 1 μM CFDA-SE at 4 °C (Vybrant™ CFDA SE Cell Tracer Kit, Thermo Fisher Scientific), that represents the control to verify CFDA-SE specificity, and one tube containing EVs was stained with the same amount of CFDA-SE at room temperature (RT) to visualize intact vesicles and set the correct dimensional gate. A mixture of fluorescent beads of varying diameters (Megamix-Plus FSC and Megamix-Plus SSC, Biocytex) suspended in filtered PBS was used following the manufacturer's instructions to discriminate EV size. Expression of typical vesicle markers CD9 (APC Mouse Anti-Human CD9, Biolegend, 312108), CD63 (PE-CyTM7 Mouse Anti-Human CD63, BD Biosciences, 561982) and CD81 (BV421 Mouse Anti-Human CD81, BD Biosciences, 740079) was evaluated within the CFDA-SE-positive events using the BD FACSAria II (BD Biosciences).

2.5. Nanoparticle Tracking Analysis (NTA) on MSC-derived EVs

EV concentrations and sizes were determined using a NanoSight LM10 instrument (Malvern Instruments Ltd, Malvern, UK) equipped with 405 nm laser and CCD camera. Readings were done as triplicates of 60 s at 30 frames per second, at a camera level set to 10 and monitoring of temperature.

2.6. Transmission electron microscopy (TEM)

MSCs were washed out in 0.1 M cacodylate buffer and immediately fixed in 0.1 M cacodylate buffer containing 2.5% glutaraldehyde (Electron Microscopy Science, Hatfield, PA, USA) for 1 h at room temperature. Cell pellets were post-fixed in osmium tetroxide for 2 h and 1% uranyl acetate for 1 h. Subsequently, samples were dehydrated through a graded ethanol series and embedded in epoxy resin (Poly-Bed; Polysciences, Inc., Warrington, PA) for 24 h at 60 °C. Ultrathin sections (50 nm) were cut and stained with 5% uranyl acetate in 50% ethanol and observed with Hitachi TEM microscope (HT7800 series, Tokyo, Japan). Electron microscopic analysis on separated vesicle preparations was performed as follows. The extracellular vesicle (EV) preparations were resuspended in 20 μl PBS (pH 7.4) and fixed by adding an equal volume of 2% paraformaldehyde in 0.1 mol/l phosphate buffer (pH 7.4). EVs were then adsorbed for 10 min to formvar-carbon coated copper grids by floating the grids on 5 μl drops on parafilm. Subsequently, grids with adhered vesicles were rinsed in PBS and negatively stained with 2% uranyl acetate for 5 min at room temperature. Stained grids were embedded in 2.5% methylcellulose for improved preservation and air dried before examination. Electron micrographs were taken at Hitachi TEM microscope (HT7800 series, Tokyo, Japan) equipped with Megaview 3 digital camera and Radius software (EMSIS, Germany). To visualize EV size distribution, the results were plotted as colorblind safe scatter dot plot in which each size measured is represented as a point along with lines for the median value and the range.

2.7. Western blot analysis

For Western blot analysis, the pre-conditioned MSCs and their corresponding separated mEVs and sEVs were resuspended in RIPA buffer (1% NONIDET p-40, 0.1% SDS, 0.1% Sodium deoxycholate, protease inhibitor cocktail 1x, in PBS pH 7.5) and protein content was quantified by BCA assay. Afterwards, 10 μg of proteins for each sample was loaded on 4–20% Mini-PROTEAN®TGX™ Precast Gel for electrophoresis, and proteins were blotted onto a PVDF membrane with a semi-dry transfer system (all from Bio-Rad Europe, Basel, Switzerland). Blot membrane was incubated overnight at 4 °C with the following specific primary antibodies: anti-syntenin (1:1000 dilution, ab133267 Abcam, USA), anti-mitofilin (1:1000 dilution, PA5 89627, Invitrogen, USA) and anti-Grp94 (1:1000 dilution, ab238126, Abcam, USA), and anti-lamin A (1:1000 dilution, ab26300, Abcam, USA) prepared in odyssey blocking buffer (LI-COR, USA) at the dilution as recommended by the manufacturer. Following, membranes were incubated with appropriate secondary antibodies such as IRDye® 680RD or 800CW goat anti-mouse or goat anti-rabbit secondary Ab (LI-COR Biosciences, Lincoln, Nebraska, USA). Infrared signal was detected using Odyssey CLx Detection System (LI-COR Biosciences).

2.8. HUVEC culture

HUVECs were plated on 1.5% (v/v) gelatin (Sigma-Aldrich, MO, USA) coated 10 cm Petri dishes and cultured in Medium 199 (Euroclone, Milan, Italy) supplemented with 10% FBS (Gibco, Milan, Italy), 2 mM L-glutamine, 50 mg/ml penicillin/streptomycin, 100 mg/ml heparin (PharmaTex, Milan, Italy), 10 μg/ml FGF-acidic, 10 μg/ml FGF-basic, 10 μg/ml EGF (Peprotech, London, UK), 1 mg/ml hydrocortisone (Sigma-Aldrich, MO, USA) (complete medium). For the described experiments, positive controls were set up with complete HUVEC medium while negative controls were set up with serum-free Medium 199 (SF). HUVECs were used at maximum passage number 5.

2.9. HUVEC proliferation assay

HUVECs were seeded at the density of $1x10^4$ cells per well on gelatin-coated 96-well plates and incubated in complete medium for 24 h to allow cell adhesion. In order to synchronize the cells before starting treatments, complete medium was replaced with SF medium for 24 h. Following, HUVECs were treated for 24 h with secretome fractions (CM, DM, mEVs and sEVs) derived from the 4 different MSC culture conditions (Nor, Hyp, Nor^{INF}, Hyp^{INF}). Cell proliferation was measured with the use of the Cell Proliferation Enzyme-linked immunosorbent assay (ELISA), Bromodeoxyuridine (BrdU) (Roche Mannheim, Germany), according to the manufacturer's instructions. Three independent experiments were performed.

2.10. HUVEC migration assay

HUVEC migration was examined using a modified Boyden chamber technique. A 24-well Transwell apparatus (Costar) was used, with each well containing a 6.5-mm polycarbonate membrane with 8 μm pores and coated with 100 μL of 1.5% (v/v) gelatin (Sigma-Aldrich, MO, USA). HUVECs (5×10^4) were placed on the membrane, and the chambers were immersed in a 24-well plate that was filled with the secretome fractions (CM, DM, mEVs and sEVs) derived from Nor, Hyp, Nor^{INF}, Hyp^{INF} conditions. After 9 h incubation, the membranes were washed briefly with PBS and the upper side of each membrane was then wiped gently with a cotton ball. Cells were fixed with methanol and the ones migrated in the lower part of the inserts were stained with Giemsa's Azur eosin methylene blue solution (10% v/v). Images were taken by Axiovert 200 M microscope (Carl Zeiss Microscopy GmbH, Jena, Germany). Images were analyzed by ImageJ with Cell Counter plug-in. Three independent experiments were performed.

2.11. Tube formation assay

Tube formation capacity by HUVECs was analyzed by using an Angiogenesis μ-slide system (Ibidi GmbH, Planegg/Martinsried, Germany). μ-slide wells were coated with growth factor reduced (GFR) Matrigel (Corning, NY, USA). After matrigel polymerization, HUVECs ($1x10^4$) were plated and incubated at 37 °C for 7 h in presence of the different secretome fractions. After incubation, cells were stained with Calcein-AM (Corning, NY, USA) and images of complete wells were taken with fluorescence microscope (Nikon Eclipse 80i, Tokyo, Japan). Images were analyzed by using Image J Software with Angiogenesis-Analyzer plug-in. Three independent experiments were performed.

2.12. Ex vivo metatarsal sprouting assay

Mice were bred and maintained at the Animal Facility of "IRCCS Ospedale Policlinico San Martino". All animal procedures were approved by the Italian Ministry of Health and by the Institutional (IRCCS Ospedale Policlinico San Martino) Ethical Committee (Authorization n. 55/2020-PR) and performed in accordance with the national current regulations regarding the protection of animals used for scientific purpose (D. Lgs. 4 Marzo 2014, n. 26, legislative transposition of Directive 2010/63/EU of the European Parliament and of the Council of September 22, 2010 on the protection of animals used for scientific purposes). The metatarsal angiogenesis assay was performed as previously described [24]. Briefly, E17.5 wild-type mice embryos (C57BL/6) were used, and metatarsal bones were isolated under stereomicroscope. Each bone was placed into 24-well plate and incubated for 96 h for bone attachment in α-MEM-Glutamax medium (GiBCo, Waltham, MA, United States), supplemented with 10% FBS (Gibco, Milan, Italy) and 50 mg/ml penicillin/streptomycin (complete medium). Complete medium was replaced with experimental secretome fractions in α-MEM-Glutamax medium supplemented with 2% FBS. While positive control was set up with complete medium, negative control was set up with 2% FBS for maintaining the fibroblast viability around the bones. After 7 days, bones were fixed and stained with rat anti-Mouse CD31 (clone SZ31) (Dianova, Hamburg, Germany). Images were captured by transmitted light microscopy using a Zeiss Axiovert 200 M microscope. CD31-positive pixels were analyzed with Image J software with vessel density plugin. Three independent experiments were performed.

2.13. Bioinformatic approach to Proteome Profiler™ Human Angiogenesis Antibody Array

The relative expression of 55 angiogenesis-related proteins were determined in CM derived from the 4 different culture conditions (Nor, Hyp, Nor^{INF}, Hyp^{INF}) by using a Proteome Profiler™ Human Angiogenesis Antibody Array (R&D Systems, Minnesota, USA) according to the manufacturer's instructions. Briefly, 30 μg of each CM derived from three independent experimental replicates were pre-incubated with the cocktail of antibodies and added onto membranes overnight at 4 °C. After several washing steps, streptavidin-horseradish peroxidase was added for 30 min and chemiluminescence of membranes was detected. Image J software with protein array analyzer plugin was used to determine the pixel density of each spot. Among 55 proteins, only the ones that were expressed at least in two independent primaries/experimental group were considered.

Statistical analyses were performed with R, under version R-3.5.1. Multivariate analysis was first carried on by dimensionality reduction on batch corrected data. Batch correction was done by considering the 3 primary donors as different batches thanks to the limma package in R. In effect, a linear model was fitted to the data, including both batches and regular treatments, then the component due to batch effects was removed. Principal components were identified by singular value decomposition as implemented in the R built-in function prcomp. To assess differentially expressed proteins between treatment conditions, MANOVA with Pillai–Bartlett statistic was applied on log10 transformed and centered scaled data without batch effect correction since the donor effect was accounted for the linear model as a blocking variable. In the one-way MANOVA, the explanatory variable was either the inflammatory status regardless of the oxygen level or the oxygen level regardless of the inflammatory status, allowing $n = 6$ observations per level. Values of $p < 0.05$ were considered statistically significant and are reported in figure's legend. Significance was also confirmed by univariate ANOVA with Bonferroni correction for multiple testing. Data distribution was evaluated on the basis of quantile–quantile (QQ) and residuals plots.

2.14. RNA preparation and next generation sequencing of EVs

mEVs and sEVs separated from MSC cultured in Nor, Hyp, Nor^{INF} and Hyp^{INF} conditions were suspended in 700 μL of Qiazol reagent (Qiagen, Limburg, the Netherlands). EV RNA was extracted with the miRNeasy Micro Kit (Qiagen) according to the manufacturer's instructions and stored at −80 °C. miRNA content was assessed by performing the Qubit® microRNA Assay Kit with the Qubit® 2.0 Fluorometer, and RNA quality and sizes were checked with Agilent 2100 Bioanalyzer (Agilent Technologies, Foster City, CA) using the Agilent Small RNA chip according to manufacturer's protocol. For RNASeq, each sequencing library was constructed from 9.2 ng of isolated miRNA. The small RNA libraries were prepared and amplified using QIAseq miRNA Library kit (Qiagen), following manufacturer's instructions. Libraries were pooled after quality check and quantification by TapeStation (Agilent Technologies, Foster City, CA) using Agilent High Sensitivity D1000 ScreenTape. Pooled libraries were quantified by real-time qPCR following "Sequencing Library qPCR Quantification" Guide (Illumina Inc., San Diego, CA) and sequenced by Illumina NextSeq platform using the 75 cycles high output kit (Illumina Inc., San Diego, CA). Data were deposited in the Gene Expression Omnibus repository (www.ncbi.nlm.nih.gov/geo/), accession number: GSE161474.

2.15. miRNAseq data analysis

FastQ data files obtained by sequencing were primarily processed by a GeneGlobe pipeline to map reads to human genome and perform Unique Molecular Indices (UMI) Analysis. Following analysis was performed on UMI-filtered reads. Differential miRNA Expression Analyses was performed using a custom R script based on Limma [25] and EdgeR [26] Bioconductor Packages. To compare the overall enrichment of miRNA species in the total vesicular RNA, miRNA reads of each sample were normalized to the miRNA fraction of total RNA. After normalization, pairwise comparisons were made according to the Limma-Voom workflow [27]. For each comparison, miRNAs emerging as outliers in volcano plots (fold change/p value scatterplots) were selected as differentially expressed, and then used to perform a hierarchical clustering of the compared samples. In case the selected miRNAs were not able to correctly classify the samples, more stringency was used for the outlier selection. Global estimates of intra-class and inter-class heterogeneity were generated analyzing the linear model fitting parameters calculated by lmFit function of Limma package. The median value of the coefficient of variation (calculated using fitting coefficients as mean values) of all miRNAs was used as intra-class heterogeneity estimate. The median absolute deviation of fold change estimates of all miRNAs, restricted to the experimental comparisons, was used as inter-class heterogeneity estimate. Given the nature of the estimates, their statistical analysis was performed by Student's t-test. Correlation matrix of miRNA expression was performed calculating Sperman correlation of the subset of miRNAs showing more variability across all samples (55% of sequenced miRNA species).

2.16. Statistical analysis

Differences in EV size revealed by flowcytometry were performed

using an unpaired two-tailed Student's *t*-test. PI/Annexin data were analyzed by two-way ANOVA. Statistical analysis of differences between multiple groups such as particle concentration, *in vitro* angiogenesis assays and *ex vivo* metatarsal assay were performed applying One-way ANOVA and Tukey's multiple comparisons test. Data are presented as mean ± SD considering at least three independent replicates for each assay and analyzed by GraphPad Prism (Graph Pad Software, Inc.). For all analyses $p < 0.05$ was considered statistically significant. In all cases: ****$p < 0.0001$, ***$p < 0.001$, **$p < 0.01$, *$p < 0.05$.

3. Results

3.1. Pre-conditioning with pro-inflammatory cytokines and hypoxia does not alter MSC properties

The main mechanism by which MSCs participate to tissue repair is through a paracrine activity and their interaction with the injured environment is a central part of this process [28]. Here, an approach based on the pre-conditioning of MSCs with pro-inflammatory cytokines and hypoxia, alone or in combination, was explored for mimicking a cellular environment more consistent with that found *in vivo*. In agreement with the guidelines of the International Society for Cell Therapy (ISCT) [29], human adipose tissue-derived MSCs grown in standard condition constitutively expressed CD29, CD44, CD73, CD90 and CD105, considered to be markers of progenitor cells of the mesenchymal lineage (Supplementary Fig. 1a). The expression of CD31, CD34 and CD45 was always less than 1%, indicating the absence of contaminating endothelial, myeloid, and hematopoietic cells (Supplementary Fig. 1a). Adipose tissue-derived MSCs possessed the ability to differentiate toward the osteogenic and adipogenic lineages (Supplementary Fig. 1b). To find out if any of the adopted pre-conditioning approaches might alter cell phenotype, the expression of the same markers was evaluated in MSCs maintained for 24 h in normoxia (Nor), hypoxia (Hyp), normoxia with inflammatory stimuli (Nor^{INF}), and hypoxia with inflammatory stimuli (Hyp^{INF}). No statistically significant differences were observed between the four treatment groups, and in comparison, with cells grown in standard condition (Supplementary Fig. 2a-d), indicating that MSCs preserve a correct immunophenotype after the 24h conditioning. Flow cytometry of Annexin V/PI-stained cells was used to quantify the apoptotic rate of MSCs exposed to serum deprivation for 24h in Nor, Hyp, Nor^{INF} and Hyp^{INF} conditions. The different pre-conditioning treatments did not alter the percentage of apoptotic, necrotic or viable cells. Only the addition of inflammatory cues to normoxic cells significantly increased the percentage of viable cells when compared to normoxia, with a concomitant decrease in the percentage of late apoptotic cells (Supplementary Fig. 1c). Taken together, these results indicate that the selected pre-conditioning approaches exerted no significant effects on the phenotype or viability of MSCs.

3.2. Preconditioned MSCs secrete EVs of different sizes

Since the cell secretome comprises a complex mixture of soluble factors and a variety of extracellular vesicles (EVs) [30], the effect of the stimulation under either normoxia or hypoxia in presence or absence of inflammatory cues was investigated on the total conditioned medium (CM), on the corresponding EV fraction, and on the so-called depleted medium (DM), that is the CM depleted of EVs (enriched only in soluble factors) (Fig. 1a). For EV separation, CM were collected from MSC-Nor, MSC-Hyp, MSC-Nor^{INF}, and MSC-Hyp^{INF} and subjected to differential ultracentrifugation. After initial low-speed centrifugation (300 x*g* and 2, 000 x*g*) to remove cells and cell debris, pelleted material recovered at medium (10,000 x*g* = 10K) centrifugation speed, enriched in medium-sized vesicles (mEVs), was washed and compared with the material pelleted at high-speed (100,000 x*g* = 100K) centrifugation, considered to be enriched in small-sized EVs (sEVs) (Fig. 1a).

Firstly, whole mounts of materials retrieved from MSCs after the 24h preconditioning and from the separated EVs (10K and 100K pellets pooled together) were analyzed by transmission electron microscopy (TEM) to obtain an overview of the heterogeneity of the secreted vesicles. TEM analysis of MSCs revealed the presence in all conditions of both multivesicular bodies (MVBs) containing smaller exosomes (Fig. 1b, left panels - black arrowheads) and larger microvesicles (MVs) budding from the plasma membrane (Fig. 1b, middle panels - black arrowheads), indicating the release of a mixed population of EVs. Images of corresponding EV pellets revealed the presence of a heterogeneous population of vesicles of different sizes ranging from 30 nm to 200 nm (Fig. 1b, right panels, red arrowheads and Fig. 1c) suggesting that the separation procedure selected a mixed population of vesicles enriched mostly, but not only, in sEVs. EVs showed round or cup-shaped morphology and were surrounded by a bilayer membrane. Smaller vesicles (30–50 nm in size) appeared round-shaped and electron-lucent (arrows), whereas larger EVs (50–200 nm) exhibited the cup-shaped morphology and appeared more electron dense (red arrowheads) (Fig. 1b, right panels).

It's well known that EVs of different sizes and intracellular origins have different functional properties [22,31]. For this reason, we analyzed separately the vesicles retrieved from the 10K (enriched in mEVs) and from the 100K pellet (enriched in sEVs). To evaluate whether mEVs and sEVs were successfully purified from Nor-CM, Hyp-CM, Nor^{INF}-CM, and Hyp^{INF}-CM, an already described non-conventional flow cytometry analysis [23] was performed. Both mEVs and sEVs were stained with the cell-permeant, fluorescein-based CFDA-SE tracer that is useful to discriminate intact vesicles from debris and membrane fragments, together with a mixture of fluorescent beads of known varying diameters (Supplementary Fig. 3a and 3b). Since CFDA-SE is able to passively diffuse within vesicles and interact with intra-vesicular enzymes at room temperature (RT) (Supplementary Fig. 3a and 3b, right panels), we ensured that at 4 °C the cloud of particles was under the level of the dimensional gate in the FL1 intensity channel (Supplementary Fig. 3a and 3b, left panels). After an accurate titration of antibodies and the use of related isotype controls [23], the expression of the typical vesicular markers CD81, CD63, CD9 belonging to the tetraspanin family was evaluated in mEVs and sEVs (Fig. 2a). Both types of vesicles expressed at different extent the three tetraspanin markers, and CD81 was the more expressed cell surface antigen in both types of MSC-derived vesicles (Fig. 2a). The diverse preconditioning strategies did not induce statistically significant differences between the two EV subpopulations (Supplementary Fig. 3c). In order to evaluate whether the material pelleted at 10K was actually enriched in mEVs compared to the 100K-retrieved material, we took advantage of the use of the above mentioned fluorescent dimensional beads (Supplementary Fig. 3a and 3b). Beads allowed to define the percentage of vesicles falling within the dimensional gate and with diameters: i) smaller than 100 nm, ii) ranging from 100 to 160 nm, and iii) from 160 to 900 nm (Fig. 2b). Our data indicate that the percentage of sEVs with a diameter smaller than 100 nm was significantly higher than the corresponding mEVs in the 4 different culture conditions (Table 1). On the contrary, the percentage of vesicles with diameters ranging from 100 to 160 nm was significantly higher in the material pelleted at 10K if compared to the 100K counterparts in all the conditions (Table 1). No main differences were observed in the few vesicles ranging from 160 to 900 nm. Only in the Hyp^{INF} condition, the percentage of mEVs bigger than 160 nm was significantly higher than the corresponding sEVs (Table 1). Nanoparticle tracking analysis (NTA) confirmed the higher representation of medium vesicles in the 10K pellet, resulting in a mean size of 225 ± 31 nm for the 10K pellet, and 170 ± 12 nm for the 100K pellet ($p = 0.0162$). Fig. 2c shows a representative NTA analysis of m- and sEVs separated from one of the three considered MSC primary cultures stimulated in normoxia. NTA showed that the concentration of mEVs and sEVs released by the same amount of MSCs did not vary significantly among the 4 different culture conditions (Fig. 2d). NTA analysis has been also performed on DM samples and their corresponding total CM. As indicated in

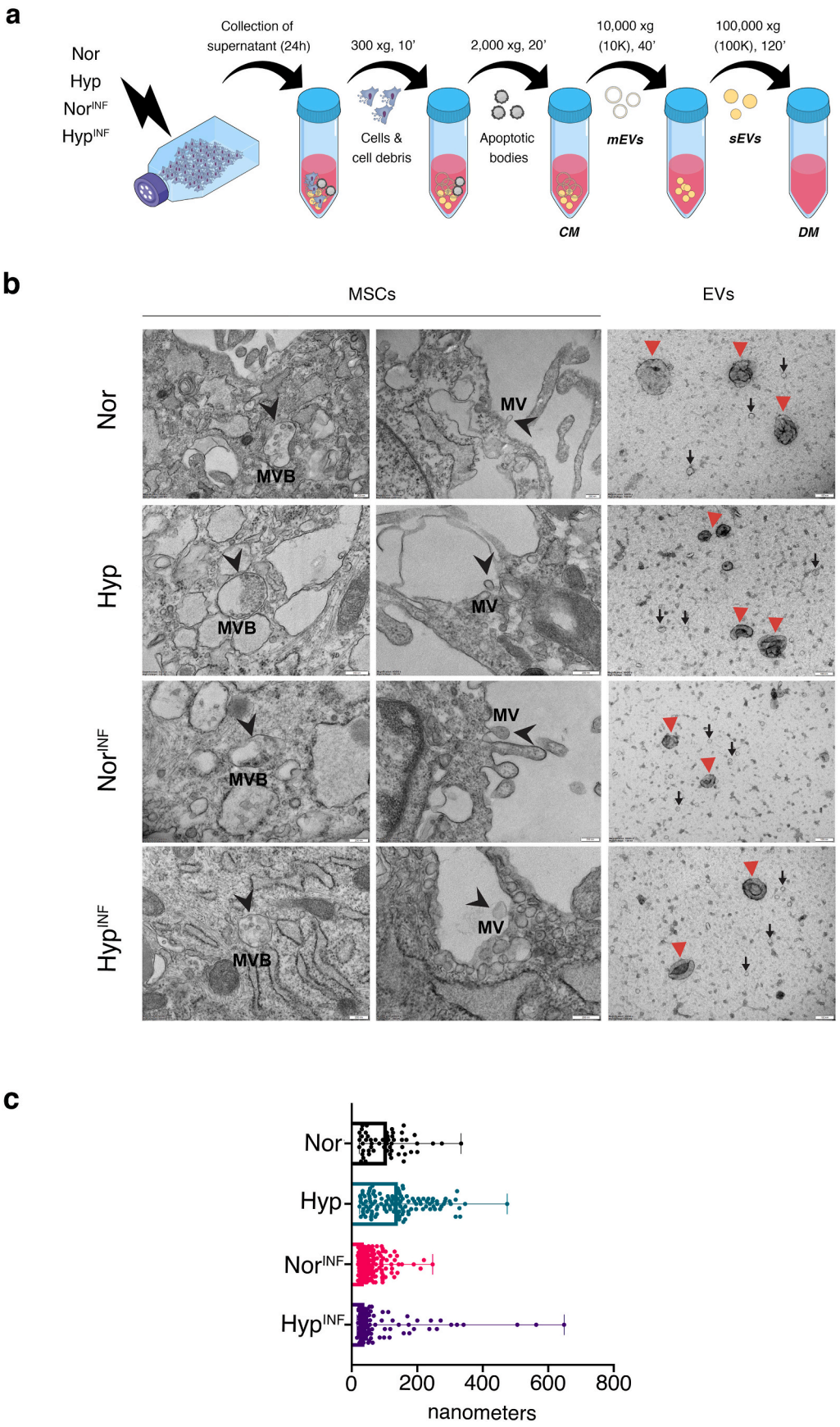

Fig. 1. Separation and characterization of MSC-derived EVs. (a) Schematic depicting the workflow used to separate the total conditioned medium (CM) and the different secretome fractions (DM, mEVs, and sEVs). (**b**) Representative TEM images of MSCs cultured in Nor, Hyp, Nor^{INF} and Hyp^{INF} conditions containing multivesicular bodies (MVB) (black arrowheads, left panels) and putative microvesicles budding from the plasma membrane (black arrowheads, middle panels). Right panels show representative TEM images of separated EVs indicating the presence of both smaller EVs (arrows) and larger EVs (red arrowheads). (**c**) TEM analysis of EV size. Data are visualized as scatter dot plot showing EV size distribution among different conditions. Each size measurement of EVs is showed as a point, whereas lines represent the median value and the range. (For interpretation of the references to color in this figure legend, the reader is referred to the Web version of this article.)

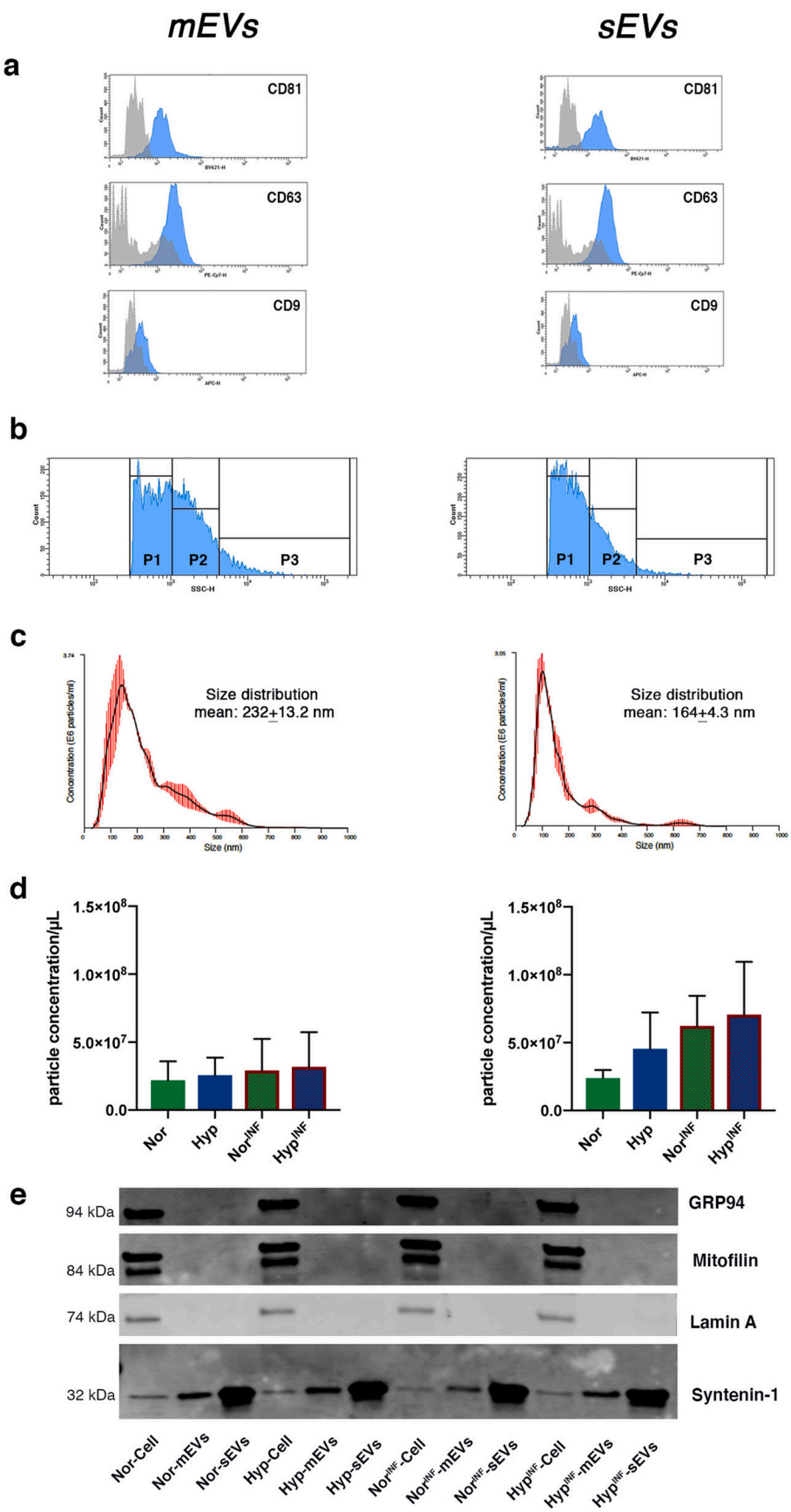

Fig. 2. Size distribution and particle concentration of EV subtypes. (a) Flow cytometry analysis of MSC-derived mEVs (left panels) and sEVs (right panels). The areas under the blue lines identify vesicles reacting with CD81, CD63, and CD9. The areas under the gray lines indicate the interactions of vesicles with corresponding nonreactive immunoglobulin of the same isotype. **(b)** Using the reference of a mixture of fluorescent beads of varying diameters, three different sub-gates can be visualized within CFSE-positive events (P1: ≤100 nm, P2: from 100 to 160 nm, P3: from 160 to 900 nm) in a SSC-H histogram. (**c**) Representative histograms showing the calculated mean ± SD of size distribution by NTA analysis of purified mEVs and sEVs. (**d**) Histograms representing the concentration/µL of mEVs and sEVs derived from the 4 preconditioning treatments (Nor, Hyp, Nor^{INF}, Hyp^{INF}). These results are based on three replicates of three independent experiments. (**e**) Western blot analysis of mEVs and sEVs and their corresponding cell lysates derived from the different preconditioning approaches (Nor, Hyp, Nor^{INF} and Hyp^{INF}). While Grp94 and Lamin A presence were observed only in cells and confirmed the non-contamination of EVs with cellular components, syntenin was mostly present mEVs and sEVs as a cytosolic EV marker. A large EV marker, Mitofilin, was expressed only in cells but it was absent in both mEVs and sEVs. (For interpretation of the references to color in this figure legend, the reader is referred to the Web version of this article.)

Table 1
Flow cytometry analysis revealing the average size of both mEVs and sEVs. Statistical analysis was performed with unpaired Student's *t*-test, considering EVs derived from three independent MSC primary cultures for each condition.

	Size	mEVS (%)	sEVS (%)	P value
	Distribution	(AVG ± SD)	(AVG ± SD)	(unpaired *t*-test)
Hyp	≤100 nm	65.45 ± 0.5710	73.27 ± 2.414	0.0344 (*)
	100–160 nm	34.54 ± 0.5710	23.38 ± 1.436	0.0020 (**)
	160–900 nm	6.213 ± 0.7044	3.143 ± 0.8827	0.0531 (ns)
Nor	≤100 nm	64.42 ± 0.7436	72.40 ± 1.524	0.0093 (**)
	100–160 nm	35.57 ± 0.7436	27.59 ± 1.524	0.0093 (**)
	160–900 nm	6.227 ± 0.7774	3.697 ± 0.6550	0.0676 (ns)
Hyp^{INF}	≤100 nm	59.11 ± 2.042	74.95 ± 2.920	0.0189 (*)
	100–160 nm	40.88 ± 2.042	25.04 ± 2.920	0.0189 (*)
	160–900 nm	7,913 ± 0.2872	2,900 ± 0.5500	0.0028 (**)
Nor^{INF}	≤100 nm	62,42 ± 0.8818	69,23 ± 1,606	0.0205 (*)
	100–160 nm	37,57 ± 0.8818	31,43 ± 2,235	0.0628 (ns)
	160–900 nm	6,997 ± 1,063	4,620 ± 0.5420	0.1172 (ns)

Supplementary Figure 3d, the percentage of total particles in DM derived from the different preconditioning strategies was significantly decreased if compared to their corresponding CM, ensuring a low interference of EVs in the later experiments. FACS and NTA analysis revealed that the EV separation procedure here adopted possessed an intermediate specificity, as already stated in the MISEV 2018 guidelines [32], and the EV sub-fractions largely overlapped.

A Western blot analysis has been performed on both mEVs and sEVs as well as on their corresponding cell lysates, derived from the different preconditioning approaches (Nor, Hyp, Nor^{INF}, and Hyp^{INF}) (Fig. 2e). We have selected Grp94 (HSP90B1) and Lamin A as proteins associated with other intracellular compartments than plasma membrane/endosomes [32]. These proteins were highly expressed by the cell lysates derived from the different preconditioning strategies, and, more importantly, they were not expressed by corresponding mEVs and sEVs, indicating that our vesicle subpopulations were not contaminated by cells. We have also evaluated the expression of Syntenin, a cytosolic protein expressed by EVs, and in particular by sEVs, as previously indicated [22,32]. We have also checked for the expression of Mitofilin, a protein anchored in the inner mitochondrial membrane, described to be expressed by large and medium-sized EVs released by dendritic cells and some tumor cell lines [22]. Mitofilin was not expressed in our MSC-derived EV subpopulations, and this could be potentially due to the different cell source (as pointed out also in the MISEV2018 paper, there could be some differences in some marker expressions due to the different cells of origin) and to the fact that we did not consider larger vesicles (2K) in our study. Taken together, these results indicate that human adipose tissue-derived MSCs release a large range of EVs, which can be partially separated by their pelleting properties.

3.3. EVs are less sensitive than soluble proteins to the environmental variations in the context of angiogenesis

The control of blood vessel growth plays a key role to restore blood supply and ensure rapid vascularization of damaged tissues [11]. To evaluate how an injured environment, here mimicked by low oxygen tension and pro-inflammatory cytokines, influences the angiogenic potential of the different MSC secretome fractions, we took in consideration different aspects of the angiogenic process: endothelial cell proliferation, migration and tubulogenesis. In order to comparatively assess the biological activity of the whole MSC secretome over the fractions within it, namely EVs and soluble factors, a known amount (in terms of protein μg) of total CM was administered according to the number of target endothelial cells in a 1:1 (cell to cell) ratio. Target cells were also stimulated by the corresponding amounts of DM, mEVs and sEVs. Firstly, the effect of the preconditioned MSC-derived secretome fractions on human umbilical vein endothelial cell (HUVEC) proliferation was investigated. CM derived from MSCs stimulated by TNF-α and IL-1α in hypoxic condition (Hyp^{INF}-CM) significantly down-regulated the proliferative capacity of responder cells when compared to its non-inflamed counterpart (Hyp^{INF}-CM vs Hyp-CM, $p \leq 0.001$) (Fig. 3a). A similar result was obtained comparing the Hyp^{INF}-DM fraction with Hyp-DM ($p \leq 0.01$), suggesting that the soluble factors released by MSCs in a hypoxic-inflamed environment inhibit the proliferation of endothelial cells (Fig. 3a). Even if BrdU incorporation by HUVECs was consistently lower in the presence of both Hyp-mEVs and Hyp-sEVs compared to the total Hyp-CM ($p \leq 0.01$ and $p \leq 0.05$, respectively), the addition of inflammatory factors in hypoxia did not affect the function of the EV fractions (Fig. 3a). On the other hand, under normoxia, only total CM were negatively affected by the addition of inflammatory stimuli, inducing a significant decrease of HUVEC proliferation (Nor-CM vs Nor^{INF}-CM, $p \leq 0.01$), without inducing major differences in DM, mEVs and sEVs (Fig. 3b). No significant differences were observed when HUVECs were incubated with the secretome fractions derived from Hyp^{INF} and Nor^{INF} conditions compared to the control medium containing TNF-α and IL-1α (only INF control condition) (Fig. 3a and b).

Since endothelial cells migrate along chemo-attractants secreted in the microenvironment, we used a transwell migration assay to create the chemical gradient by putting secretome fractions in the lower chamber. Even if Hyp-CM and -DM induced a strong HUVEC migration compared to Nor-CM and -DM ($p \leq 0.0001$ and $p \leq 0.001$, respectively) (Supplementary Fig. 3f), none of the hypoxic secretome fractions prevailed in inducing HUVEC migration (Supplementary Fig. 3f). Similarly to the effects observed in the proliferation assay, MSCs activated by the inflammatory cytokines in hypoxic condition produced a total CM and DM that negatively affected the migratory capacity of HUVECs compared to their corresponding non-inflamed counterparts (Hyp-CM vs Hyp^{INF}-CM, $p \leq 0.0001$; Hyp-DM vs Hyp^{INF}-DM, $p \leq 0.01$) (Fig. 3c). The presence of the inflammatory mediators did not affect the migratory capacity induced by the hypoxic EV fractions (Fig. 3c). In normoxia, the EV fractions, and in particular sEVs, are the main components responsible for the generation of a gradient to which HUVECs migrate (Nor-DM vs Nor-sEVs, $p \leq 0.001$) (Fig. 3d), but in this case the addition of inflammation did not significantly alter neither the capacity of the total CM nor the ability of DM and mEVs to induce HUVEC migration (Fig. 3d). Only sEVs effect was significantly down regulated (Nor-sEVs vs Nor^{INF}-sEVs, $p \leq 0.01$). The presence of TNF-α and IL-1α in control medium (only INF control group) did not exert any significant migratory effect on HUVEC (Fig. 3c and d).

Assays that simulate the formation of capillary-like tubules are regarded as representative of the later stages of angiogenesis. A tube formation assay was used as a quick high-throughput screen to evaluate the role of the secretome fractions on this specific aspect of the angiogenic process. The quantitative analysis of total branch numbers showed that under hypoxia, MSCs released secretomes that induced the formation of vessel like structures (Fig. 3e and f). Interestingly, inflammatory mediators added to hypoxia exerted a significant inhibitory effect on the capacity of total CM and related secretome fractions to induce the formation of tube-like structures by HUVECs (Hyp-CM vs Hyp^{INF}-CM, $p \leq 0.01$; Hyp-DM vs Hyp^{INF}-DM, $p \leq 0.05$; Hyp-mEVs vs Hyp^{INF}-mEVs, $p \leq 0.01$; Hyp-sEVs vs Hyp^{INF}-sEVs, $p \leq 0.0001$) (Fig. 3e and f). A similar trend was observed in the normoxic counterparts, even if a significant difference was observed only when considering the mEVs fraction (Nor-mEVs vs Nor^{INF}-mEVs, $p \leq 0.01$) (Fig. 3g). Taken together, these results indicate that the synergistic action of hypoxia and inflammation affects the MSC secretome fractions to different extents. The ability of soluble factors to induce HUVEC proliferation, migration and differentiation is significantly impaired. On the contrary, the ability of the EV fractions to induce endothelial cell proliferation and migration is not affected, while the capacity of promoting the formation of tube-like structures is significantly impaired.

To confirm the *in vitro* results, the mouse fetal metatarsal sprouting

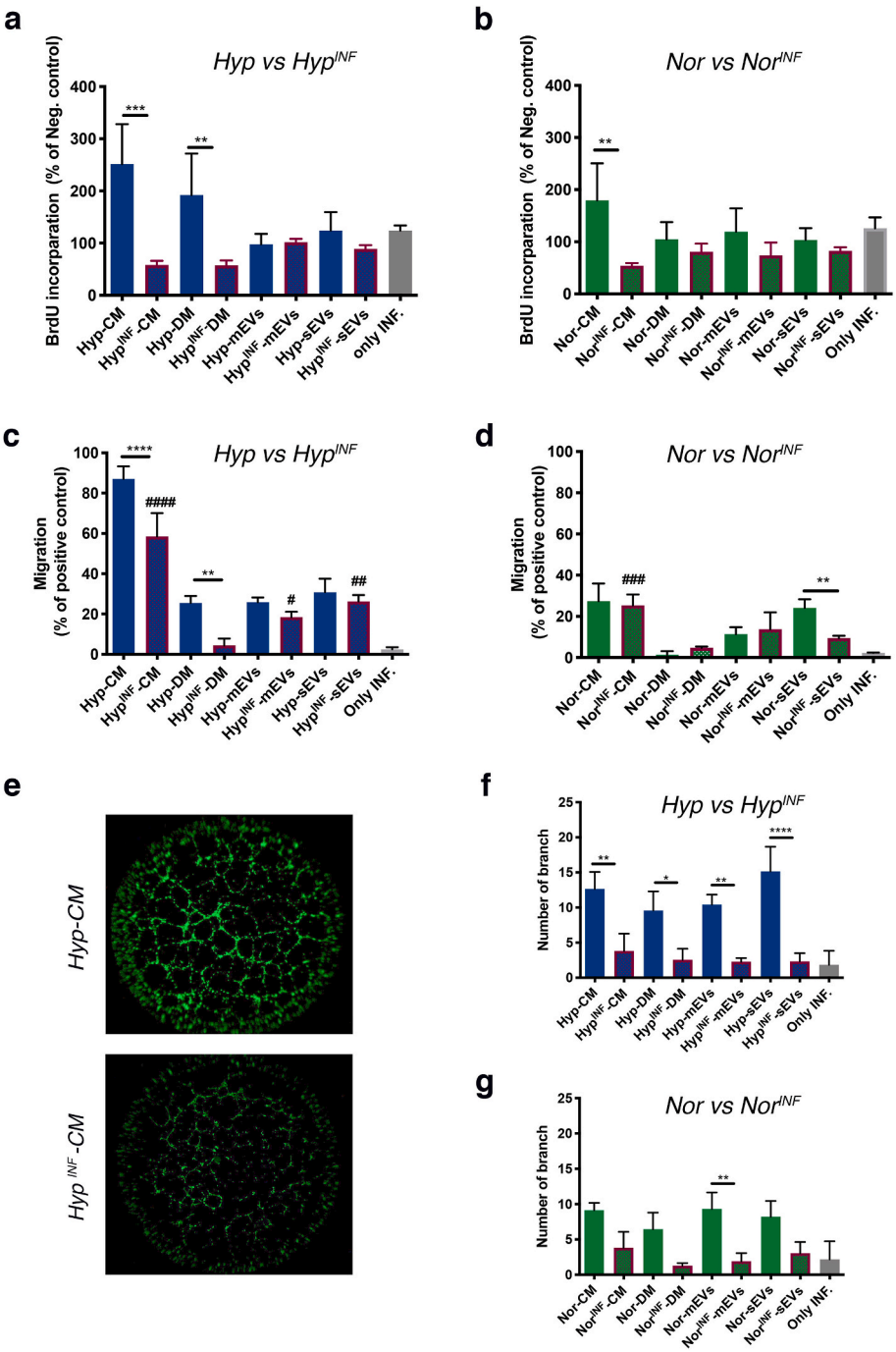

Fig. 3. The effect of MSC secretome fractions on proliferation, migration and tube formation capacity of HUVECs. (a, b) Proliferation was determined with BrdU incorporation assay. (**c, d**) Cell migration was determined by transwell migration assay. (**e**) Representative images of Calcein AM staining of HUVECs at 7th hour on GFR-Matrigel. (**f, g**) Quantitative analysis of number of branches in tube formation assay. Error bars in the graphs represent mean ± SD. N = 3, (*) presents the statistical differences between the groups, while (#) presents the difference from the control "only-INF" experimental group. ****$p < 0.0001$, ***$p < 0.001$, **$p < 0.01$, *$p < 0.05$, $^{\#\#\#\#}p < 0.0001$, $^{\#\#\#}p < 0.001$, $^{\#\#}p < 0.01$, $^{\#}p < 0.05$ (one-way ANOVA and Tukey multiple comparison).

assay was selected, since it provides an exceptional tool for studying angiogenesis [24]. In comparison with other commonly used *in vitro* or *ex vivo* angiogenesis assays, vessel outgrowth from mouse fetal metatarsals is more representative of sprouting angiogenesis *in vivo*. It allows the analysis of blood vessel growth with CD31 staining and the mechanisms underpinning this process, in a multicellular microenvironment that drives the formation of a robust and complex vascular network (Fig. 4a). The soluble factors released by MSCs stimulated with hypoxia and inflammation inhibited significantly the sprouting of $CD31^+$ vessels, if compared to the hypoxic counterparts (Hyp-CM vs Hyp^{INF}-CM, $p \leq 0.001$; Hyp-DM vs Hyp^{INF}-DM, $p \leq 0.05$) (Fig. 4b and c). The vessel sprouting induced by EV fractions, and in particular by sEVs, were not affected by the inhibitory effect given by the synergistic action of hypoxia and inflammation, but rather they induced a significant increase in vessel sprouting compared to their corresponding soluble factors (Hyp^{INF}-DM vs Hyp^{INF}-sEVs, $p \leq 0.01$) (Fig. 4c). In normoxia, the addition of inflammatory cytokines negatively affected only the total CM (Nor-CM vs Nor^{INF}-CM, $p \leq 0.01$), while the effects exerted by the secretome fractions were not significantly affected (Fig. 4d). In this assay, the inflammatory cytokines in the control medium (only-INF group) induced a significant increase in vessel density if compared to Hyp^{INF}-CM and Hyp^{INF}-DM ($p \leq 0.05$ and $p \leq 0.01$, respectively) (Fig. 4c), as well as to Nor^{INF}-CM and Nor^{INF}-DM ($p \leq 0.05$ and $p \leq 0.01$, respectively) (Fig. 4d), suggesting that inflammation-activated MSCs release soluble factors that counteract the angiogenic capacity induced by TNF-α and IL-1α.

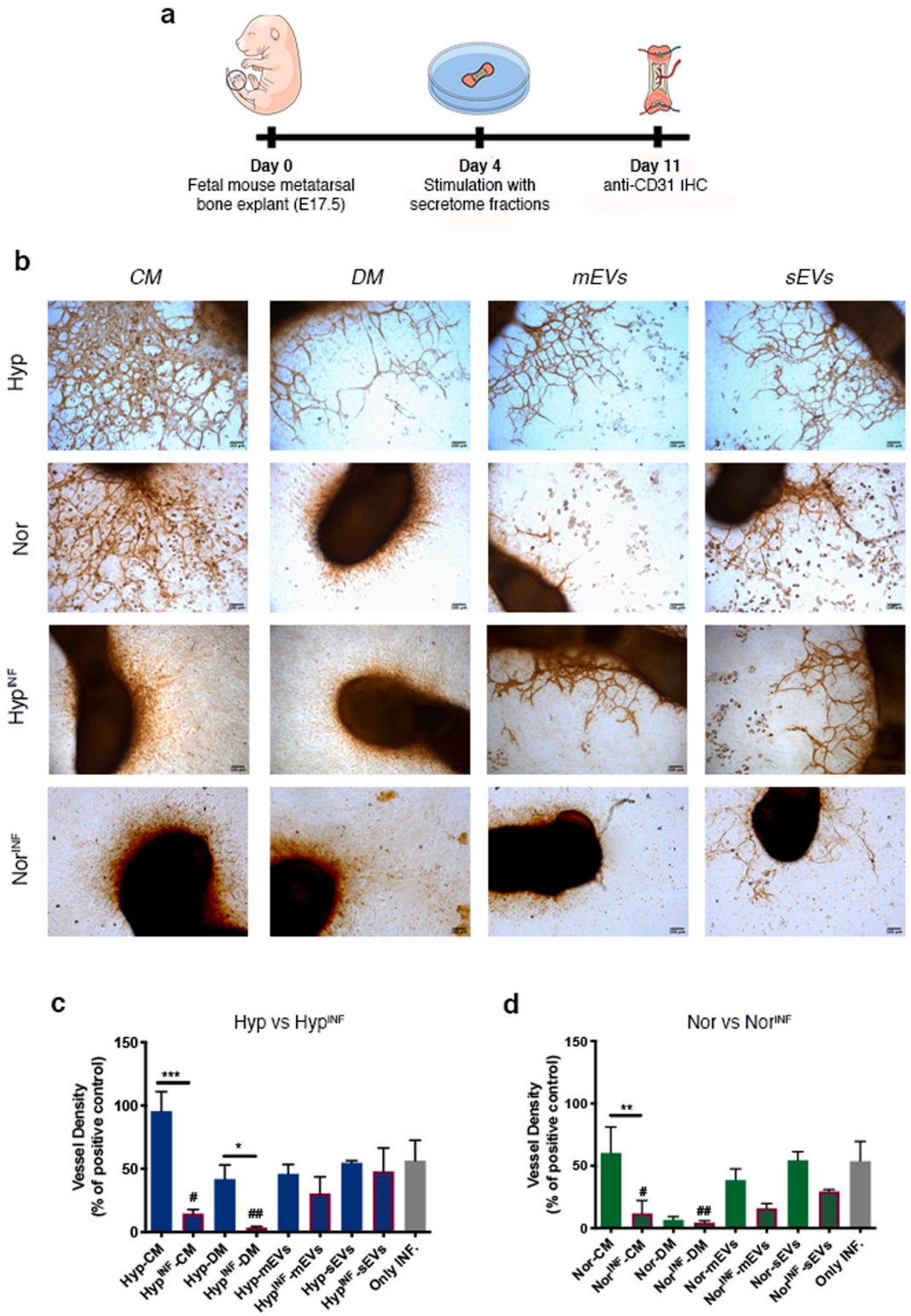

Fig. 4. Ex vivo metatarsal sprouting assay. (a) Schematic diagram of the experimental plan, illustrating the timeline of the isolation of metatarsals, secretome stimulation and anti-CD31 staining. (**b**) Representative image of $CD31^{+}$ vessel structures, scale bar:100 μm. (**c, d**) Quantitative analysis of vessel density, CD31-positive cells were considered for the analysis. Error bars in the graphs represent mean ± SD. N = 3, (*) presents the statistical differences between the groups, while (#) presents the difference from the control "only-INF" experimental group. ****$p < 0.0001$, ***$p < 0.001$, **$p < 0.01$, *$p < 0.05$, $^{\#\#}p < 0.01$, $^{\#}p < 0.05$ (one-way ANOVA and Tukey multiple comparison).

3.4. Soluble factors released by inflammation-activated MSCs possess a distinctive secretome profile

The *in vitro* and *ex vivo* analysis above described indicated that inflammation-activated MSCs secreted proteins that inhibited angiogenesis if compared to their non-stimulated counterparts.

To define the profile of the soluble mediators secreted by MSCs, we examined and compared the CM derived from cells stimulated in Nor, Hyp, Nor^{INF} and Hyp^{INF} conditions using a human protein cytokine array. Donor origin of the samples explained most of the variance in the dataset. In order to understand how preconditioning strategies drive the principal components (PC) of the analyzed dataset in the principal component analysis (PCA) and provide the overall structure of the effect of inflammation and hypoxia, donor effect was evaluated and removed with the limma package of R [25] and data distribution has been evaluated (Supplementary Fig. 4a and 4b).

Based on the amount of secreted proteins, samples that underwent inflammation can be clearly separated from the non-inflamed ones along the first component (PC1) of the PCA, which explained 43.5% of the variance (Fig. 5a and b).

When we analyzed the effects of inflammation, regardless of the oxygen levels, we observed a significant up-regulation in the expression of proteins, such as: i) Granulocyte-Macrophage Colony-Stimulating Factor (GM-CSF) and Monocyte Chemoattractant Protein-1 (MCP-1), involved not only in the recruitment of monocytes/macrophages, but also whose presence is of basic importance in the repair process [33,34]; ii) Heparin-Binding Epidermal growth factor–like Growth Factor (HB-EGF), whose level increases in response to different forms of injuries as well as stimuli, acting as a critical mediator of tissue repair and regeneration [35]; iii) Matrix Metalloproteinase-8 and -9, enzymes implicated in the degradation of most of the extracellular matrix components and therefore actively involved in tissue remodeling associated with pathological situations such as acute injury [36] (Fig. 5e). The contribution of each protein to the different components of the PCA further confirmed that the above-mentioned proteins (MMPs, MCP-1, GM-CSF, etc.) were among the main positive drivers of PC1 (Fig. 5c). On the other hand, when a similar bioinformatic approach was performed to evidence the effects of hypoxia, regardless of inflammation, the most characterizing and significantly expressed proteins were: i) Endoglin, an auxillary TGF-beta receptor that modulates TGF-beta 1 and beta 3 responses and plays a role in vascular development, angiogenesis and vascular remodeling [37]; ii) Hepatocyte Growth Factor (HGF), a pro-angiogenic factor that exert a striking effect on endothelial cell migration, therefore playing a crucial role in recruiting endothelial cells *in vivo* for the formation of new blood vessels [38]; iii) Vascular Endothelial Growth Factor (VEGF), a well known signal protein that stimulates the formation of blood vessels [39]; Urokinase-type Plasminogen Activator (uPA), described to be involved in endothelial cell proliferation, migration and tubule formation [40] (Fig. 5e). Regarding the PCA, samples that underwent hypoxic treatment could separate from the normoxic ones mainly along the second component, which explained 16.7% of the variance (Fig. 5d). uPA, VEGF, and Endoglin were also important contributors of PC2 (Fig. 5d). Of note, although some proteins, such as DPPIV and Coagulation Factor 3, were main drivers of PC2, they were not differentially expressed due to oxygen levels from the statistical point of view. This is due to the fact that PC1 also explained a small part of the variance between hypoxic and normoxic observations, as shown by the spread of the samples in the PCs space (Fig. 5a and d). The proteins majorly contributing to PC1 and PC2 were also expressed by the corresponding DM derived from the different preconditioning strategies (Supplementary Fig. 4c).

Taken together, these results indicate that there is a set of soluble mediators generated by MSCs in a milieu-specific manner, responding to the requirements of the environment.

3.5. The microRNA (miRNA) landscape of MSC-derived EVs is not majorly affected by cell preconditioning

Small RNAs within EVs are thought to be major contributors to the molecular events occurring in the recipient cell [41]. We evaluated whether the adopted preconditioning strategies had affected the RNA cargo within both mEVs and sEVs. Capillary electrophoresis profiling on vesicular RNA revealed distinctive peaks around 20 and 70 nucleotides, suggestive of the presence of miRNAs and tRNAs (Supplementary Fig. 5a). To better define and compare the small RNA composition of the differently preconditioned MSC-derived EV fractions, we performed RNA sequencing of vesicular RNA. The sequencing yielded a total of 192 million reads, and the technical consistency was validated measuring the correlation between technical replicates, which proved to be higher than the one of biological replicates (Supplementary Fig. 5c). The levels of the most variable miRNAs across all samples were used to perform a hierarchical clustering. The two generated main clusters nicely separate mEV and sEV subfractions with only few exceptions (Supplementary Fig. 5b).

Cargo RNAs of both mEVs and sEVs include various biotypes that represent a selected portion of the RNA content of the source cell. Indeed, the libraries of both EV fractions were highly enriched in the classes of: i) rRNAs (46.5% in mEVs and 43.5% in sEVs), tRNAs (11.0% in mEVs and 20.1% in sEVs) and mRNAs (1.1% in mEVs and 0.7% in sEVs), that can be considered as possible non-functional degradation products; ii) miRNAs (7.7% in mEVs and 11.7% in sEVs), that have been established to be functional when carried by EVs between cells; iii) piRNAs (1.4% in mEVs and 2.2% in sEVs), that are predicted to be functional but have not been definitively demonstrated to mediate intercellular communication [42] (Fig. 6a). Although miRNAs represent a small fraction of all RNA species found in EVs (Fig. 6a), an exponentially growing number of new reports indicate that a great part of the EV effects can be attributed to their miRNA content [43–45]. Interestingly, the relative distribution of miRNA species was uneven, with few miRNAs extremely more enriched than others. In particular, 65.5% and 71% of total miRNA reads in mEVs and sEVs respectively was accounted by only 15 highly enriched miRNA species (Fig. 6b and c and Supplementary Fig. 6). We therefore focused on the 15 top enriched miRNAs characterizing both m- and sEVs from each culture condition (Nor, Hyp, Nor^{INF} and Hyp^{INF}), unexpectedly identifying a group of only 18 miRNAs. Indeed, 13 out of 18 miRNAs are shared by all the considered experimental groups, indicating that their prevalence is independent of cell preconditioning and EV sub-fractioning (Fig. 6d). We also observed that let-7a-5p and miR-26a-5p are shared by mEVs, while miR-125a-5p is shared by sEVs, suggesting a possible role in discriminating the two MSC-derived EV subsets (Fig. 6d). We asked wether a global miRNome analysis could unveil any modulation of miRNA signatures, likely belonging to the lowly enriched ones. Most of the differences were observed comparing mEVs derived from differently conditioned MSCs, while sEVs presented few differentially enriched miRNAs (Fig. 7a). Of note, the differentially enriched (DE) miRNAs didn't correspond to the top expressed ones (Supplementary Fig. 7). Addition of inflammatory stimuli, regardless of oxygen level, induced a characteristic signature in both m- and sEVs, when compared to non-inflamed counterparts (Supplementary Fig. 7). The most significant outlier miRNA present in both EV subtypes upon inflammation and hypoxia is miR-146a-5p, described to modulate the expression of pro-inflammatory genes, thus reducing or delaying inflammation and enhancing wound healing [46,47] (Supplementary Fig. 7). Given the lower number of DE miRNAs in sEVs, we hypothesized that their miRNA composition could be more homogeneous than mEVs among the culture conditions. To test this hypothesis, we evaluated whether the lower amount of DE miRNAs was due to lower inter-class heterogeneity or higher intra-class heterogeneity (noise). No significant differences in terms of intra-class heterogeneity were observed between sEVs and mEVs, while the inter-class heterogeneity was significantly lower among sEV classes (Fig. 7b). Consistently,

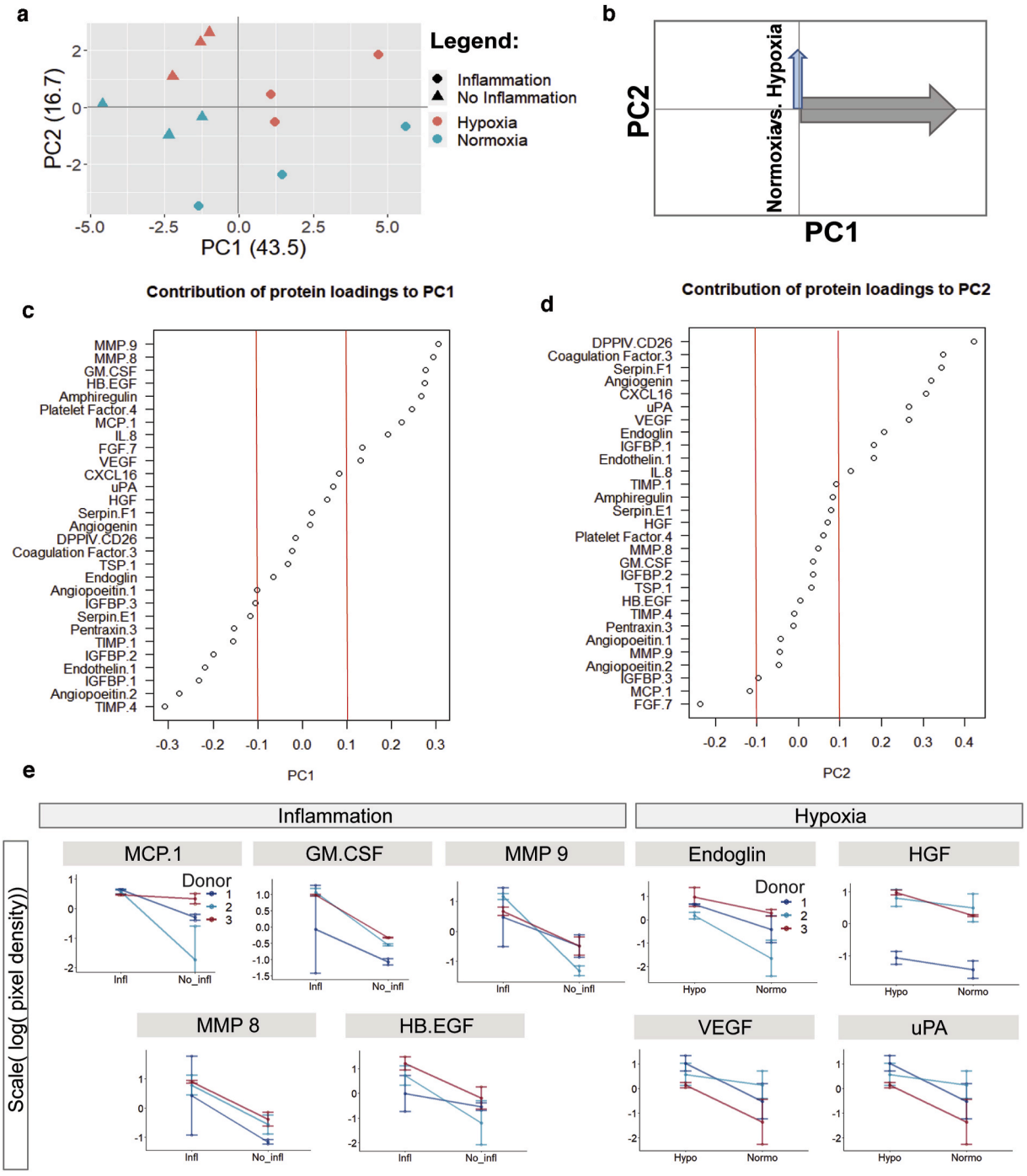

Fig. 5. Treatment conditions are successfully separated by singular value decomposition and trigger changes in protein expressions. (a) Samples are separated in the principal component analysis with PC1 and PC2 explaining 43.5% and 16.7% of the variance, respectively. (**b**) Schematic summary: based on the response loadings, PC1 is mainly driven by the inflammatory status while PC2 can be defined by the oxygen influence. (**c, d**) Visualization of proteins associated with reduction components and ordered from the most negative contribution to the most positive contribution to PC1 and PC2, respectively. Red dashed lines are arbitrary thresholds (±0.1) set to visualize most important protein contributions. (**e**) Most of the proteins had significantly different levels between donors. Log10 transformed and normalized pixel densities for each protein are represented as a proxy of protein expression on the y-axis. Average and standard error are calculated between normoxia and hypoxia in inflammation (INF) versus conditions without inflammation (No-INF), for each donor. The expression of five proteins was significantly increased (MMP-9: $p = 0.005$, MMP-8: $p = 0.01$, GM-CSF: $p = 0.012$, HB-EGF = 0.018, MCP-1: $p = 0.04$) for the inflammation influence regardless of oxygen levels in MANOVA. The expression of four proteins was significantly increased (Endoglin: $p = 0.009$, HGF: $p = 0.039$, VEGF: $p = 0.031$, uPA: $p = 0.043$). for the oxygen level influence regardless of the inflammatory status in MANOVA. Only proteins with $p < 0.05$ are reported. (For interpretation of the references to color in this figure legend, the reader is referred to the Web version of this article.)

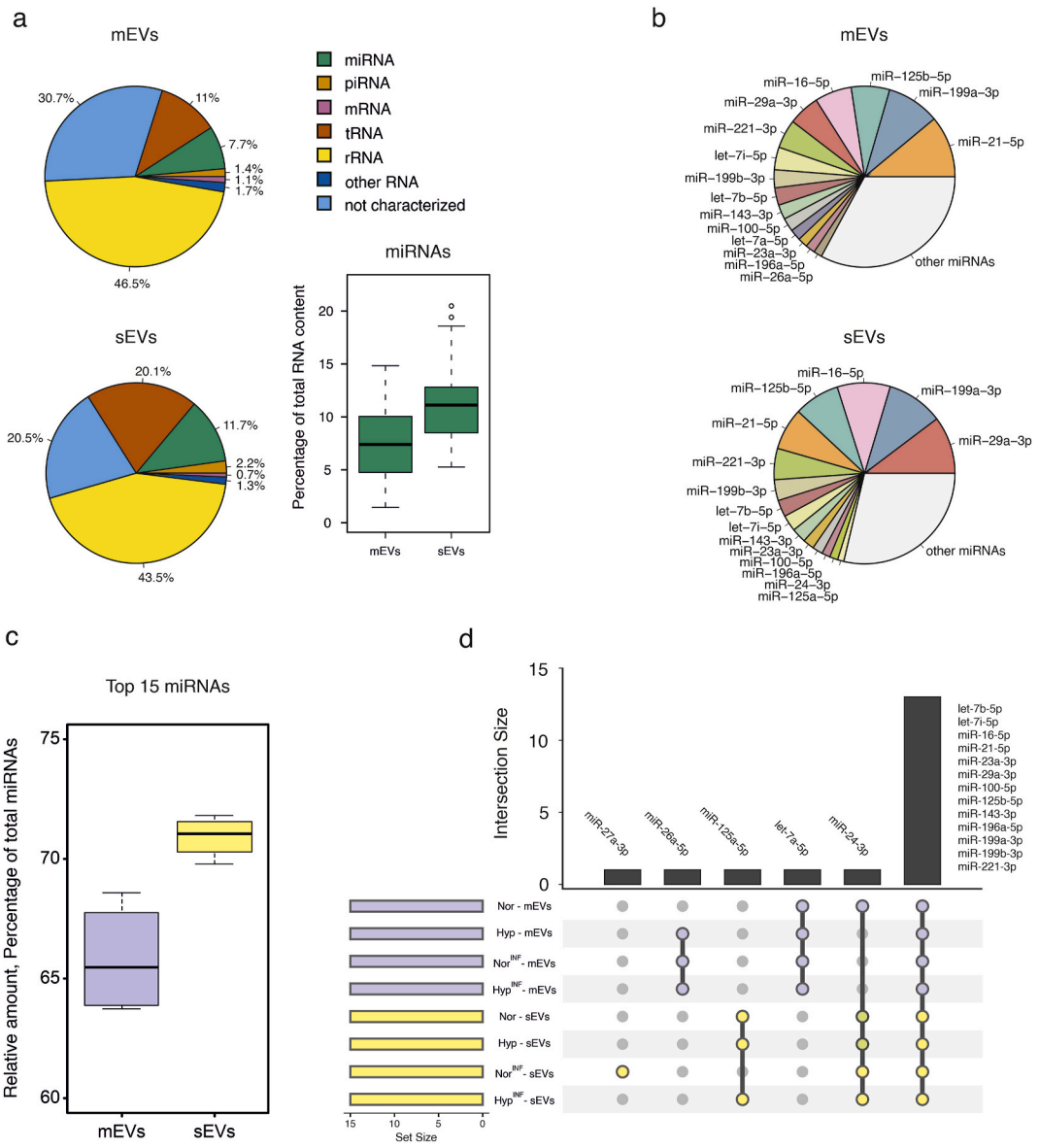

Fig. 6. Few enriched miRNAs cover the majority of EV miRNA content and are shared by different treatment conditions. (a) Relative distribution of retrieved RNA types in mEVs and sEVs. Slices of piecharts represent average values. Boxplot shows the distribution of miRNA percentages in all the samples. (**b**) Relative distribution of miRNA species in mEVs and sEVs. Colored slices of piecharts represent the amount of the 15 most enriched miRNAs in the samples. (**c**) Percentage of total miRNA content covered in each sample by its 15 most enriched miRNA species. (**d**) Upset plot shows miRNA species which are enriched regardless of treatment conditions and EV sub-fractioning.

correlation analysis provided further evidence that sEVs miRNome is globally less affected by environmental changes than the one of mEVs (Fig. 7c).

4. Discussion

MSC-sourced secretome consists of soluble and EV-encapsulated components, whose synergistic action is able to reduce cell injury and improve tissue repair capacity [48]. Indeed, cells release heterogeneous vesicles of different sizes and intracellular origins, including small EVs generated in the endosomal compartments (i.e., exosomes) and EVs of various sizes budding from the plasma membrane, generally referred to as microvesicles [49]. A large number of MSC-derived bioactive molecules containing genetic material (DNA, RNA fragments, miRNAs) are enveloped within extracellular vesicles [42]. It has been reported that the composition of the MSC secretome can be regulated by preconditioning strategies during the culture *in vitro* [6]. An appropriate preconditioning may prepare the cells to release factors that could better respond to the harsh environment present at the site of injury, characterized by strong inflammation and low oxygen supply [50]. Several approaches have been investigated so far, and a variety of different factors has been proven to modulate the MSC therapeutic capacity, including 3D culture [51,52], pharmacological molecules [53,54], inflammatory cytokines [55,56], and hypoxia [6,57]. This study shows for the first time the effects of a simultaneous stimulation with pro-inflammatory cytokines (TNF-α and IL-1α) and hypoxia (1% O_2) on the different components of the MSC secretome. These cytokines were selected being able to induce endothelial cells to express adhesion molecules and chemokines that attract white cells from the blood to the site of injury [58]. Thus, four different culture conditions were considered: the normoxic environment (20% O_2) (Nor) was regarded as the control condition and compared to a hypoxic one (Hyp), with or without the simultaneous stimulation with the inflammatory cytokines (Nor^{INF} and Hyp^{INF}, respectively). We observed that the environmental

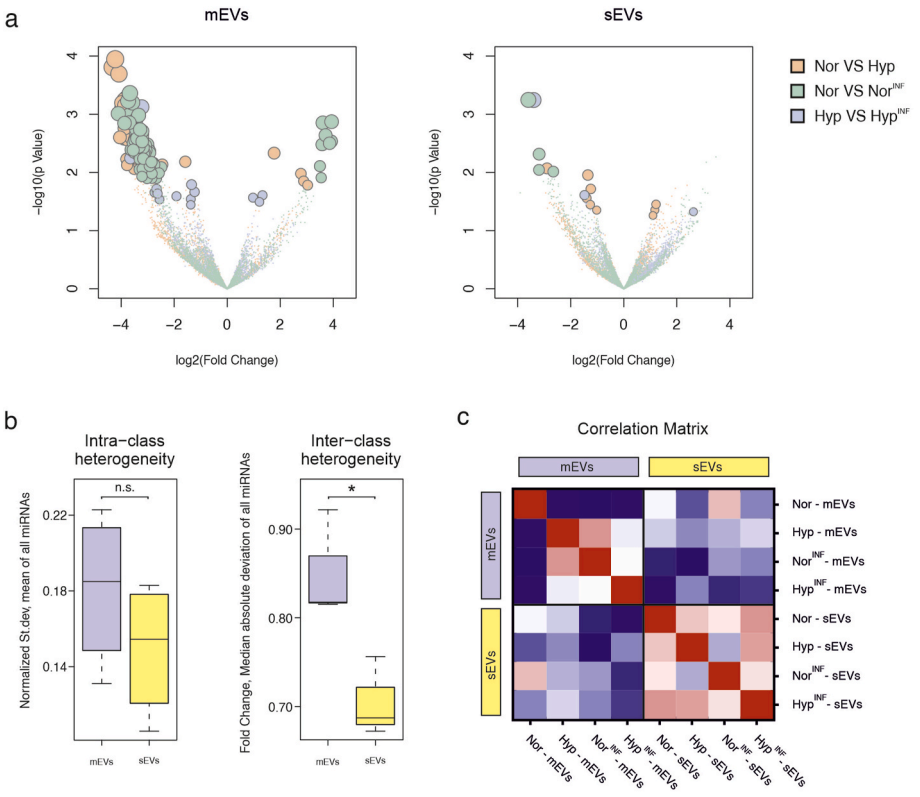

Fig. 7. Differential expression analysis reveals sEVs are more homogeneous than mEVs in miRNA content. (a) Volcano plots show miRNAs enriched in EVs derived from differently treated cells. (**b**) Boxplots compare the intra-class and inter-class heterogeneity estimators of mEVs and sEVs. (**c**) Correlation matrix of EV groups, based on Spearman correlation of miRNA levels. *p < 0.05 (Student's *t*-test).

variations strongly influenced the angiogenic potential of the MSC secretomes. Several literature reports indicate that MSC secretome can exert different effects in the context of angiogenesis, and many of these differences largely depends upon the various culture conditions [12,13]. Although MSCs have historically been reported to be an interesting source of pro-angiogenic factors, recent studies indicate that MSCs can also exert detrimental effects on endothelial cell function. These discrepancies could be ascribed to a multitude of reasons, ranging from the isolation techniques, the species from which MSC populations have originated, the cell source (bone marrow, adipose tissue, umbilical cord), the passage number, and, last but not least, the adopted preconditioning strategy. In particular, the activation of MSCs with inflammatory cytokines have been reported to induce opposite effects in the context of angiogenesis. Adipose tissue-derived MSCs stimulated with 10 ng/ml TNF-α produced a conditioned medium (CM) able to stimulate the homing and engraftment of endothelial progenitors in a hindlimb ischemia mouse model [17]. Moreover, treatments with CM derived from TNF-α preconditioned MSCs have been described to accelerate cutaneous wound healing and angiogenesis *in vivo* [59]. On the contrary, recent literature reports have demonstrated that, once activated by a pro-inflammatory environment (given by a cocktail composed by 25 ng/ml IL1b, 20 ng/ml IL6, 25 ng/ml TNF-α), the total conditioned medium derived from both human and mouse bone marrow-MSCs exerted strong anti-angiogenic effects [18,60]. The same group has recently demonstrated that the extracellular vesicles produced by MSCs activated by the same cocktail of inflammatory cytokines inhibited angiogenesis targeting both ECM remodeling and endothelial cell migration [19]. Here, we demonstrated that when human adipose tissue-derived MSCs were licensed by hypoxia and by 50 ng/ml TNF-α and 50 ng/ml IL-1α, they produced a total CM that significantly inhibited the proliferation, migration and tubulogenesis of responder endothelial cells, as well as the sprouting capacity of $CD31^+$ cells in an *ex vivo* fetal mouse metatarsal sprouting assay. Surprisingly, when we deeply investigated these effects in the secretome fractions composing the total CM, namely EVs and soluble proteins, interesting differences emerged. Indeed, the pro-angiogenic capacity of the soluble component of the MSC secretome was significantly inhibited, regardless of the oxygen level, if compared to the non-inflamed counterparts. On the contrary, the EV-encapsulated component was not strongly affected by the inflammatory stimuli, suggesting a different capacity of the secretome fractions to sense the environmental variations. When MSCs were licensed by inflammation, they reacted increasing significantly the release of proteins such as GM-CSF, MCP-1, MMP-8, MMP-9, and HB-EGF, involved mainly in the interaction with the innate immune system, as well as in tissue remodeling and repair [61]. MSCs exposed to hypoxia modulated the expression of proteins (Endoglin, HGF, VEGF, and uPA) implicated, to different extents, in the angiogenic process, confirming previously reported data [20,62,63]. A great part of the EV effects is due to their miRNA content [64–66]. Interestingly, miRNA profiling of both medium- and small-EVs released by preconditioned MSCs revealed that the relative distribution of miRNA species was unbalanced, with few (15) miRNAs accounting for almost two-thirds of the total miRNA content. More importantly, the top enriched miRNAs were shared not only by the small and medium vesicles belonging to the same experimental group, but also by the different preconditioning strategies. We also observed that the differentially enriched miRNAs did not correspond to the top expressed ones, and the most significant outlier present in both EV subtypes upon inflammation and hypoxia was miR-146a-5p, described to modulate the expression of pro-inflammatory genes, thus reducing or delaying inflammation and enhance wound healing [46,67].

In conclusion, this study provides insight into the capacity of the different MSC secretome fractions to respond to the different environmental variations. Our results highlight the importance of not only selecting the appropriate preconditioning strategy to alter properly the release of paracrine factors, but also the relevance of considering

separately the effects that such approaches could induce on either the soluble or EV-encapsulated components of the cell secretome. Future studies will need to focus on developing standardize protocols among the scientific community to establish preconditioning regimes useful to enhance the regenerative capacities of MSC therapies.

5. Data availability

All relevant data supporting the findings of this study are available within the paper, its supplementary information and from the corresponding authors upon reasonable request.

Author contribution

C.G. Conceptualization, Methodology, Investigation, Data curation, Visualization, Formal analysis, Writing – original draft, preparation; D. C. Investigation and Data curation of RNAseq data, Visualization, Formal analysis, Writing – original draft, preparation; R.L. Data curation of proteomic data, Visualization, Formal analysis, Writing – original draft, preparation; F.V. Investigation of cDNA libraries; D.R. Investigation and Data curation of flow cytometry data; C.B. Investigation and Data curation of Nanoparticle Tracking Analysis and Western Blot; S.S. Investigation and Data curation of TEM images; K.C. Investigation, Data curation and Visualization and Writing – original draft; P.M. Investigation and Data curation, Resources; L.G. Data curation of proteomic data, Visualization, Formal analysis, Resources; R.Q. Writing – review & editing and Resources; R.T. Conceptualization, Methodology, Visualization, Formal analysis, Writing – original draft, preparation, Supervision, Funding acquisition. All authors approved the submission of the manuscript.

Declaration of competing interest

The authors declare that they have no known competing financial interests or personal relationships that could have appeared to influence the work reported in this paper.

Acknowledgments

This project has received funding from the European Union's Horizon 2020 research and innovation programme under Marie Sklodowska-Curie grant agreement No. 721432 CarBon to C.G., R.L, L.G and R.T.

Appendix A. Supplementary data

Supplementary data to this article can be found online at https://doi.org/10.1016/j.biomaterials.2020.120633.

References

[1] A.M. DiMarino, A.I. Caplan, T.L. Bonfield, Mesenchymal stem cells in tissue repair, Front. Immunol. 4 (2013) 201, https://doi.org/10.3389/fimmu.2013.00201.
[2] S. Eleuteri, A. Fierabracci, Insights into the secretome of mesenchymal stem cells and its potential applications, Int. J. Mol. Sci. 20 (2019) 4597, https://doi.org/10.3390/ijms20184597.
[3] M.F. Pittenger, D.E. Discher, B.M. Péault, D.G. Phinney, J.M. Hare, A.I. Caplan, Mesenchymal stem cell perspective: cell biology to clinical progress, Npj Regen. Med. 4 (2019) 1–15, https://doi.org/10.1038/s41536-019-0083-6.
[4] C. Hu, L. Li, Preconditioning influences mesenchymal stem cell properties *in vitro* and *in vivo*, J. Cell Mol. Med. 22 (2018) 1428–1442, https://doi.org/10.1111/jcmm.13492.
[5] S. A, O. V, N. T, J. M, C. Wc, Preconditioning of human mesenchymal stem cells to enhance their regulation of the immune response, Stem Cell. Int. (2016), https://doi.org/10.1155/2016/3924858.
[6] N.D.C. Noronha Nc, A. Mizukami, C. Caliári-Oliveira, J.G. Cominal, J.L.M. Rocha, D.T. Covas, K. Swiech, K.C.R. Malmegrim, Priming approaches to improve the efficacy of mesenchymal stromal cell-based therapies, Stem Cell Res. Ther. 10 (2019), https://doi.org/10.1186/s13287-019-1224-y.
[7] W.X. Hong, M.S. Hu, M. Esquivel, G.Y. Liang, R.C. Rennert, A. McArdle, K.J. Paik, D. Duscher, G.C. Gurtner, H.P. Lorenz, M.T. Longaker, The role of hypoxia-inducible factor in wound healing, Adv. Wound Care 3 (2014) 390–399, https://doi.org/10.1089/wound.2013.0520.
[8] R.J. Ruthenborg, J.J. Ban, A. Wazir, N. Takeda, J.W. Kim, Regulation of wound healing and fibrosis by hypoxia and hypoxia-inducible factor-1, Mol. Cell. 37 (2014) 637–643, https://doi.org/10.14348/molcells.2014.0150.
[9] A.S. MacLeod, J.N. Mansbridge, The innate immune system in acute and chronic wounds, Adv. Wound Care 5 (2016) 65–78, https://doi.org/10.1089/wound.2014.0608.
[10] X.L. Fan, Y. Zhang, X. Li, Q.L. Fu, Mechanisms underlying the protective effects of mesenchymal stem cell-based therapy, Cell. Mol. Life Sci. 77 (2020) 2771–2794, https://doi.org/10.1007/s00018-020-03454-6.
[11] R. Gianni-Barrera, N. Di Maggio, L. Melly, M.G. Burger, E. Mujagic, L. Gürke, D. J. Schaefer, A. Banfi, Therapeutic vascularization in regenerative medicine, stem cells transl, Med 9 (2020) 433–444, https://doi.org/10.1002/sctm.19-0319.
[12] H.M. Kwon, S.M. Hur, K.Y. Park, C.K. Kim, Y.M. Kim, H.S. Kim, H.C. Shin, M. H. Won, K.S. Ha, Y.G. Kwon, D.H. Lee, Y.M. Kim, Multiple paracrine factors secreted by mesenchymal stem cells contribute to angiogenesis, Vasc. Pharmacol. 63 (2014) 19–28, https://doi.org/10.1016/j.vph.2014.06.004.
[13] S.J. Marfy-Smith, C.E. Clarkin, Are mesenchymal stem cells so bloody great after all? Stem Cells Transl. Med. 6 (2017) 3–6, https://doi.org/10.5966/sctm.2016-0026.
[14] L. Liu, J. Gao, Y. Yuan, Q. Chang, Y. Liao, F. Lu, Hypoxia preconditioned human adipose derived mesenchymal stem cells enhance angiogenic potential via secretion of increased VEGF and bFGF, Cell Biol. Int. 37 (2013) 551–560, https://doi.org/10.1002/cbin.10097.
[15] J.R. Ferreira, G.Q. Teixeira, S.G. Santos, M.A. Barbosa, G. Almeida-Porada, R. M. Gonçalves, Mesenchymal stromal cell secretome: influencing therapeutic potential by cellular pre-conditioning, Front. Immunol. 9 (2018), https://doi.org/10.3389/fimmu.2018.02837.
[16] L. Zhao, C. Hu, P. Zhang, H. Jiang, J. Chen, Preconditioning strategies for improving the survival rate and paracrine ability of mesenchymal stem cells in acute kidney injury, J. Cell Mol. Med. 23 (2019) 720–730, https://doi.org/10.1111/jcmm.14035.
[17] Y.W. Kwon, S.C. Heo, G.O. Jeong, J.W. Yoon, W.M. Mo, M.J. Lee, I.H. Jang, S. M. Kwon, J.S. Lee, J.H. Kim, Tumor necrosis factor-α-activated mesenchymal stem cells promote endothelial progenitor cell homing and angiogenesis, Biochim. Biophys. Acta (BBA) - Mol. Basis Dis. 1832 (2013) 2136–2144, https://doi.org/10.1016/j.bbadis.2013.08.002.
[18] E. Maffioli, S. Nonnis, R. Angioni, F. Santagata, B. Calì, L. Zanotti, A. Negri, A. Viola, G. Tedeschi, Proteomic analysis of the secretome of human bone marrow-derived mesenchymal stem cells primed by pro-inflammatory cytokines, J. Proteomics. 166 (2017) 115–126, https://doi.org/10.1016/j.jprot.2017.07.012.
[19] R. Angioni, C. Liboni, S. Herkenne, R. Sánchez-Rodríguez, G. Borile, E. Marcuzzi, B. Calì, M. Muraca, A. Viola, CD73+ extracellular vesicles inhibit angiogenesis through adenosine A2B receptor signalling, J. Extracell. Vesicles 9 (2020), https://doi.org/10.1080/20013078.2020.1757900.
[20] C. Lo Sicco, D. Reverberi, C. Balbi, V. Ulivi, E. Principi, L. Pascucci, P. Becherini, M. C. Bosco, L. Varesio, C. Franzin, M. Pozzobon, R. Cancedda, R. Tasso, Mesenchymal stem cell-derived extracellular vesicles as mediators of anti-inflammatory effects: endorsement of macrophage polarization, Stem Cells Transl. Med. 6 (2017) 1018–1028, https://doi.org/10.1002/sctm.16-0363.
[21] J. Van Deun, P. Mestdagh, P. Agostinis, Ö. Akay, S. Anand, J. Anckaert, Z. A. Martinez, T. Baetens, E. Beghein, L. Bertier, G. Berx, J. Boere, S. Boukouris, M. Bremer, D. Buschmann, J.B. Byrd, C. Casert, L. Cheng, A. Cmoch, D. Daveloose, E. De Smedt, S. Demirsoy, V. Depoorter, B. Dhondt, T.A.P. Driedonks, A. Dudek, A. Elsharawy, I. Floris, A.D. Foers, K. Gärtner, A.D. Garg, E. Geeurickx, J. Gettemans, F. Ghazavi, B. Giebel, T.G. Kormelink, G. Hancock, H. Helsmoortel, A.F. Hill, V. Hyenne, H. Kalra, D. Kim, J. Kowal, S. Kraemer, P. Leidinger, C. Leonelli, Y. Liang, L. Lippens, S. Liu, A. Lo Cicero, S. Martin, S. Mathivanan, P. Mathiyalagan, T. Matusek, G. Milani, M. Monguió-Tortajada, L.M. Mus, D. C. Muth, A. Németh, E.N.M. Nolte-'T Hoen, L. O'Driscoll, R. Palmulli, M.W. Pfaffl, B. Primdal-Bengtson, E. Romano, Q. Rousseau, S. Sahoo, N. Sampaio, M. Samuel, B. Scicluna, B. Soen, A. Steels, J.V. Swinnen, M. Takatalo, S. Thaminy, C. Théry, J. Tulkens, I. Van Audenhove, S. Van Der Grein, A. Van Goethem, M.J. Van Herwijnen, G. Van Niel, N. Van Roy, A.R. Van Vliet, N. Vandamme, S. Vanhauwaert, G. Vergauwen, F. Verweij, A. Wallaert, M. Wauben, K.W. Witwer, M.I. Zonneveld, O. De Wever, J. Vandesompele, A. Hendrix, EV-TRACK: transparent reporting and centralizing knowledge in extracellular vesicle research, Nat. Methods 14 (2017), https://doi.org/10.1038/nmeth.4185.
[22] J. Kowal, G. Arras, M. Colombo, M. Jouve, J.P. Morath, B. Primdal-Bengtson, F. Dingli, D. Loew, M. Tkach, C. Théry, Proteomic comparison defines novel markers to characterize heterogeneous populations of extracellular vesicle subtypes, Proc. Natl. Acad. Sci. U. S. A 113 (2016) E968–E977, https://doi.org/10.1073/pnas.1521230113.
[23] C. Gorgun, D. Reverberi, G. Rotta, F. Villa, R. Quarto, R. Tasso, Isolation and flow cytometry characterization of extracellular-vesicle subpopulations derived from human mesenchymal stromal cells, Curr. Protoc. Stem Cell Biol. 48 (2019) e76, https://doi.org/10.1002/cpsc.76.
[24] W. Song, C.W. Fhu, K.H. Ang, C.H. Liu, N.A.B. Johari, D. Lio, S. Abraham, W. Hong, S.E. Moss, J. Greenwood, X. Wang, The fetal mouse metatarsal bone explant as a model of angiogenesis, Nat. Protoc. 10 (2015) 1459–1473, https://doi.org/10.1038/nprot.2015.097.
[25] M. Ritchie, B. Phipson, D. Wu, Y. Hu, C.W. Law, W. Shi, G.K. Smyth, Limma Powers Differential Expression Analyses for RNA-Sequencing and Microarray Studies, vol. 43, Nucleic Acids Research, Oxford Academic, 2015, p. e47. https://doi:10.1093/nar/gkv007.

[26] M.D. Robinson, D.J. McCarthy, G.K. Smyth, edgeR: a Bioconductor package for differential expression analysis of digital gene expression data, Bioinformatics 26 (2010) 139–140. https://doi: 10.1093/bioinformatics/btp616.
[27] C.W. Law, Y. Chen, W. Shi, G.K. Smyth, Voom: precision weights unlock linear model analysis tools for RNA-seq read counts, Genome Biol. 15 (2014) R29, https://doi.org/10.1186/gb-2014-15-2-r29.
[28] G. Qiu, G. Zheng, M. Ge, J. Wang, R. Huang, Q. Shu, J. Xu, Mesenchymal stem cell-derived extracellular vesicles affect disease outcomes via transfer of microRNAs, Stem Cell Res. Ther. 9 (2018) 1–9, https://doi.org/10.1186/s13287-018-1069-9.
[29] M. Dominici, K. Le Blanc, I. Mueller, I. Slaper-Cortenbach, F.C. Marini, D.S. Krause, R.J. Deans, A. Keating, D.J. Prockop, E.M. Horwitz, Minimal criteria for defining multipotent mesenchymal stromal cells. The International Society for Cellular Therapy position statement, Cytotherapy 8 (2006) 315–317, https://doi.org/10.1080/14653240600855905.
[30] R. Mitchell, B. Mellows, J. Sheard, M. Antonioli, O. Kretz, D. Chambers, M.-T. Zeuner, J.E. Tomkins, B. Denecke, L. Musante, B. Joch, F. Debacq-Chainiaux, H. Holthofer, S. Ray, T.B. Huber, J. Dengjel, P. De Coppi, D. Widera, K. Patel, Secretome of adipose-derived mesenchymal stem cells promotes skeletal muscle regeneration through synergistic action of extracellular vesicle cargo and soluble proteins, Stem Cell Res. Ther. 10 (2019) 116, https://doi.org/10.1186/s13287-019-1213-1.
[31] A. Zijlstra, D. Di Vizio, Size matters in nanoscale communication, Nat. Cell Biol. 20 (2018) 228–230, https://doi.org/10.1038/s41556-018-0049-8.
[32] C. Théry, K.W. Witwer, E. Aikawa, M.J. Alcaraz, J.D. Anderson, R. Andriantsitohaina, A. Antoniou, T. Arab, F. Archer, G.K. Atkin-Smith, D.C. Ayre, J.M. Bach, D. Bachurski, H. Baharvand, L. Balaj, S. Baldacchino, N.N. Bauer, A. A. Baxter, M. Bebawy, C. Beckham, A. Bedina Zavec, A. Benmoussa, A.C. Berardi, P. Bergese, E. Bielska, C. Blenkiron, S. Bobis-Wozowicz, E. Boilard, W. Boireau, A. Bongiovanni, F.E. Borràs, S. Bosch, C.M. Boulanger, X. Breakefield, A.M. Breglio, M. Brennan, D.R. Brigstock, A. Brisson, M.L.D. Broekman, J.F. Bromberg, P. Bryl-Górecka, S. Buch, A.H. Buck, D. Burger, S. Busatto, D. Buschmann, B. Bussolati, E. I. Buzás, J.B. Byrd, G. Camussi, D.R.F. Carter, S. Caruso, L.W. Chamley, Y.T. Chang, A.D. Chaudhuri, C. Chen, S. Chen, L. Cheng, A.R. Chin, A. Clayton, S.P. Clerici, A. Cocks, E. Cocucci, R.J. Coffey, A. Cordeiro-da-Silva, Y. Couch, F.A.W. Coumans, B. Coyle, R. Crescitelli, M.F. Criado, C. D'Souza-Schorey, S. Das, P. de Candia, E. F. De Santana, O. De Wever, H.A. del Portillo, T. Demaret, S. Deville, A. Devitt, B. Dhondt, D. Di Vizio, L.C. Dieterich, V. Dolo, A.P. Dominguez Rubio, M. Dominici, M.R. Dourado, T.A.P. Driedonks, F.V. Duarte, H.M. Duncan, R. M. Eichenberger, K. Ekström, S. EL Andaloussi, C. Elie-Caille, U. Erdbrügger, J. M. Falcón-Pérez, F. Fatima, J.E. Fish, M. Flores-Bellver, A. Försönits, A. Frelet-Barrand, F. Fricke, G. Fuhrmann, S. Gabrielsson, A. Gámez-Valero, C. Gardiner, K. Gärtner, R. Gaudin, Y.S. Gho, B. Giebel, C. Gilbert, M. Gimona, I. Giusti, D.C. I. Goberdhan, A. Görgens, S.M. Gorski, D.W. Greening, J.C. Gross, A. Gualerzi, G. N. Gupta, D. Gustafson, A. Handberg, R.A. Haraszti, P. Harrison, H. Hegyesi, A. Hendrix, A.F. Hill, F.H. Hochberg, K.F. Hoffmann, B. Holder, H. Holthofer, B. Hosseinkhani, G. Hu, Y. Huang, V. Huber, S. Hunt, A.G.E. Ibrahim, T. Ikezu, J. M. Inal, M. Isin, A. Ivanova, H.K. Jackson, S. Jacobsen, S.M. Jay, M. Jayachandran, G. Jenster, L. Jiang, S.M. Johnson, J.C. Jones, A. Jong, T. Jovanovic-Talisman, S. Jung, R. Kalluri, S. ichi Kano, S. Kaur, Y. Kawamura, E.T. Keller, D. Khamari, E. Khomyakova, A. Khvorova, P. Kierulf, K.P. Kim, T. Kislinger, M. Klingeborn, D. J. Klinke, M. Kornek, M.M. Kosanović, Á.F. Kovács, E.M. Krämer-Albers, S. Krasemann, M. Krause, I.V. Kurochkin, G.D. Kusuma, S. Kuypers, S. Laitinen, S. M. Langevin, L.R. Languino, J. Lannigan, C. Lässer, L.C. Laurent, G. Lavieu, E. Lázaro-Ibáñez, S. Le Lay, M.S. Lee, Y.X.F. Lee, D.S. Lemos, M. Lenassi, A. Leszczynska, I.T.S. Li, K. Liao, S.F. Libregts, E. Ligeti, R. Lim, S.K. Lim, A. Linē, K. Linnemannstöns, A. Llorente, C.A. Lombard, M.J. Lorenowicz, Á.M. Lörincz, J. Lötvall, J. Lovett, M.C. Lowry, X. Loyer, Q. Lu, B. Lukomska, T.R. Lunavat, S.L. N. Maas, H. Malhi, A. Marcilla, J. Mariani, J. Mariscal, E.S. Martens-Uzunova, L. Martin-Jaular, M.C. Martinez, V.R. Martins, M. Mathieu, S. Mathivanan, M. Maugeri, L.K. McGinnis, M.J. McVey, D.G. Meckes, K.L. Meehan, I. Mertens, V. R. Minciacchi, A. Möller, M. Møller Jørgensen, A. Morales-Kastresana, J. Morhayim, F. Mullier, M. Muraca, L. Musante, V. Mussack, D.C. Muth, K. H. Myburgh, T. Najrana, M. Nawaz, I. Nazarenko, P. Nejsum, C. Neri, T. Neri, R. Nieuwland, L. Nimrichter, J.P. Nolan, E.N.M. Nolte-'t Hoen, N. Noren Hooten, L. O'Driscoll, T. O'Grady, A. O'Loghlen, T. Ochiya, M. Olivier, A. Ortiz, L.A. Ortiz, X. Osteikoetxea, O. Ostegaard, M. Ostrowski, J. Park, D.M. Pegtel, H. Peinado, F. Perut, M.W. Pfaffl, D.G. Phinney, B.C.H. Pieters, R.C. Pink, D.S. Pisetsky, E. Pogge von Strandmann, I. Polakovicova, I.K.H. Poon, B.H. Powell, I. Prada, L. Pulliam, P. Quesenberry, A. Radeghieri, R.L. Raffai, S. Raimondo, J. Rak, M. I. Ramirez, G. Raposo, M.S. Rayyan, N. Regev-Rudzki, F.L. Ricklefs, P.D. Robbins, D.D. Roberts, S.C. Rodrigues, E. Rohde, S. Rome, K.M.A. Rouschop, A. Rughetti, A. E. Russell, P. Saá, S. Sahoo, E. Salas-Huenuleo, C. Sánchez, J.A. Saugstad, M. J. Saul, R.M. Schiffelers, R. Schneider, T.H. Schøyen, A. Scott, E. Shahaj, S. Sharma, O. Shatnyeva, F. Shekari, G.V. Shelke, A.K. Shetty, K. Shiba, P.R.M. Siljander, A. M. Silva, A. Skowronek, O.L. Snyder, R.P. Soares, B.W. Sódar, C. Soekmadji, J. Sotillo, P.D. Stahl, W. Stoorvogel, S.L. Stott, E.F. Strasser, S. Swift, H. Tahara, M. Tewari, K. Timms, S. Tiwari, R. Tixeira, M. Tkach, W.S. Toh, R. Tomasini, A. C. Torrecilhas, J.P. Tosar, V. Toxavidis, L. Urbanelli, P. Vader, B.W.M. van Balkom, S.G. van der Grein, J. Van Deun, M.J.C. van Herwijnen, K. Van Keuren-Jensen, G. van Niel, M.E. van Royen, A.J. van Wijnen, M.H. Vasconcelos, I.J. Vechetti, T. D. Veit, L.J. Vella, É. Velot, F.J. Verweij, B. Vestad, J.L. Viñas, T. Visnovitz, K. V. Vukman, J. Wahlgren, D.C. Watson, M.H.M. Wauben, A. Weaver, J.P. Webber, V. Weber, A.M. Wehman, D.J. Weiss, J.A. Welsh, S. Wendt, A.M. Wheelock, Z. Wiener, L. Witte, J. Wolfram, A. Xagorari, P. Xander, J. Xu, X. Yan, M. Yáñez-Mó, H. Yin, Y. Yuana, V. Zappulli, J. Zarubova, V. Žėkas, J. ye Zhang, Z. Zhao, L. Zheng, A.R. Zheutlin, A.M. Zickler, P. Zimmermann, A.M. Zivkovic, D. Zocco, E. K. Zuba-Surma, Minimal information for studies of extracellular vesicles 2018 (MISEV2018): a position statement of the International Society for Extracellular Vesicles and update of the MISEV2014 guidelines, J. Extracell. Vesicles 7 (2018), https://doi.org/10.1080/20013078.2018.1535750.
[33] A. Mann, K. Niekisch, P. Schirmacher, M. Blessing, Granulocyte-macrophage colony-stimulating factor is essential for normal wound healing, J. Invest. Dermatol. Symp. Proc. 11 (2006) 87–92, https://doi.org/10.1038/sj.jidsymp.5650013.
[34] S. Wood, V. Jayaraman, E.J. Huelsmann, B. Bonish, D. Burgad, G. Sivaramakrishnan, S. Qin, L.A. DiPietro, A. Zloza, C. Zhang, S.H. Shafikhani, Pro-inflammatory chemokine CCL2 (MCP-1) promotes healing in diabetic wounds by restoring the macrophage response, PloS One 9 (2014), e91574, https://doi.org/10.1371/journal.pone.0091574.
[35] D.T. Dao, L. Anez-Bustillos, R.M. Adam, M. Puder, D.R. Bielenberg, Heparin-binding epidermal growth factor–like growth factor as a critical mediator of tissue repair and regeneration, Am. J. Pathol. 188 (2018) 2446–2456, https://doi.org/10.1016/j.ajpath.2018.07.016.
[36] M. Corbel, E. Boichot, V. Lagente, Role of gelatinases MMP-2 and MMP-9 in tissue remodeling following acute lung injury, Braz. J. Med. Biol. Res. 33 (2000) 749–754, https://doi.org/10.1590/S0100-879X2000000700004.
[37] J.M. López-Novoa, C. Bernabeu, The physiological role of endoglin in the cardiovascular system, Am. J. Physiol. Heart Circ. Physiol. 299 (2010) 959–974, https://doi.org/10.1152/ajpheart.01251.2009.
[38] A.J. Braga Osorio Gomes Salgado, R.L. Goncalves Reis, N. Jorge Carvalho Sousa, J. M. Gimble, A.J. Salgado, R.L. Reis, N. Sousa, Adipose tissue derived stem cells secretome: soluble factors and their roles in regenerative medicine, Curr. Stem Cell Res. Ther. 5 (2010) 103–110, https://doi.org/10.2174/157488810791268564.
[39] M. Shibuya, Vascular endothelial growth factor (VEGF) and its receptor (VEGFR) signaling in angiogenesis: a crucial target for anti- and pro-angiogenic therapies, Genes and Cancer 2 (2011) 1097–1105, https://doi.org/10.1177/1947601911423031.
[40] V. Stepanova, P.S. Jayaraman, S.V. Zaitsev, T. Lebedeva, K. Bdeir, R. Kershaw, K. R. Holman, Y.V. Parfyonova, E.V. Semina, I.B. Beloglazova, V.A. Tkachuk, D. B. Cines, Urokinase-type plasminogen activator (upa) promotes angiogenesis by attenuating proline-rich homeodomain protein (prh) transcription factor activity and de-repressing vascular endothelial growth factor (vegf) receptor expression, J. Biol. Chem. 291 (2016) 15029–15045, https://doi.org/10.1074/jbc.M115.678490.
[41] A. Turchinovich, O. Drapkina, A. Tonevitsky, Transcriptome of extracellular vesicles: state-of-the-art, Front. Immunol. 10 (2019) 202, https://doi.org/10.3389/fimmu.2019.00202.
[42] K. O'Brien, K. Breyne, S. Ughetto, L.C. Laurent, X.O. Breakefield, RNA delivery by extracellular vesicles in mammalian cells and its applications, Nat. Rev. Mol. Cell Biol. (2020) 1–22, https://doi.org/10.1038/s41580-020-0251-y.
[43] X. Chen, H. Liang, J. Zhang, K. Zen, C.Y. Zhang, Secreted microRNAs: a new form of intercellular communication, Trends Cell Biol. 22 (2012) 125–132, https://doi.org/10.1016/j.tcb.2011.12.001.
[44] H. Valadi, K. Ekström, A. Bossios, M. Sjöstrand, J.J. Lee, J.O. Lötvall, Exosome-mediated transfer of mRNAs and microRNAs is a novel mechanism of genetic exchange between cells, Nat. Cell Biol. 9 (2007) 654–659, https://doi.org/10.1038/ncb1596.
[45] N. Kosaka, H. Iguchi, Y. Yoshioka, F. Takeshita, Y. Matsuki, T. Ochiya, Secretory mechanisms and intercellular transfer of microRNAs in living cells, J. Biol. Chem. 285 (2010) 17442–17452, https://doi.org/10.1074/jbc.M110.107821.
[46] D. Ti, H. Hao, X. Fu, W. Han, Mesenchymal stem cells-derived exosomal microRNAs contribute to wound inflammation, Sci. China Life Sci. 59 (2016) 1305–1312, https://doi.org/10.1007/s11427-016-0240-4.
[47] J. Hamanishi, M. Mandai, N. Matsumura, T. Baba, K. Yamaguchi, S. Fujii, I. Konishi, Activated local immunity by CC chemokine ligand 19-transduced embryonic endothelial progenitor cells suppresses metastasis of murine ovarian cancer, Stem Cell. 28 (2010) 164–173, https://doi.org/10.1002/stem.256.
[48] C. Harrell, C. Fellabaum, N. Jovicic, V. Djonov, N. Arsenijevic, V. Volarevic, Molecular mechanisms responsible for therapeutic potential of mesenchymal stem cell-derived secretome, Cells 8 (2019) 467, https://doi.org/10.3390/cells8050467.
[49] G. Raposo, W. Stoorvogel, Extracellular vesicles: exosomes, microvesicles, and friends, J. Cell Biol. 200 (2013) 373–383, https://doi.org/10.1083/jcb.201211138.
[50] L. Chen, H. Deng, H. Cui, J. Fang, Z. Zuo, J. Deng, Y. Li, X. Wang, L. Zhao, Inflammatory responses and inflammation-associated diseases in organs, Oncotarget 9 (2018) 7204–7218, https://doi.org/10.18632/oncotarget.23208.
[51] T.J. Bartosh, J.H. Ylöstalo, A. Mohammadipoor, N. Bazhanov, K. Coble, K. Claypool, R.H. Lee, H. Choi, D.J. Prockop, Aggregation of human mesenchymal stromal cells (MSCs) into 3D spheroids enhances their antiinflammatory properties, Proc. Natl. Acad. Sci. U. S. A 107 (2010) 13724–13729, https://doi.org/10.1073/pnas.1008117107.
[52] B. Follin, M. Juhl, S. Cohen, A.E. Perdersen, J. Kastrup, A. Ekblond, Increased paracrine immunomodulatory potential of mesenchymal stromal cells in three-dimensional culture, Tissue Eng. B Rev. 22 (2016) 322–329, https://doi.org/10.1089/ten.teb.2015.0532.
[53] X. Cui, H. Wang, H. Guo, C. Wang, H. Ao, X. Liu, Y.Z. Tan, Transplantation of mesenchymal stem cells preconditioned with diazoxide, a mitochondrial ATP-sensitive potassium channel opener, promotes repair of myocardial infarction in rats, Tohoku J. Exp. Med. 220 (2010) 139–147, https://doi.org/10.1620/tjem.220.139.
[54] A. Pessina, V. Coccè, L. Pascucci, A. Bonomi, L. Cavicchini, F. Sisto, M. Ferrari, E. Ciusani, A. Crovace, M.L. Falchetti, S. Zicari, A. Caruso, S. Navone, G. Marfia,

A. Benetti, P. Ceccarelli, E. Parati, G. Alessandri, Mesenchymal stromal cells primed with Paclitaxel attract and kill leukaemia cells, inhibit angiogenesis and improve survival of leukaemia-bearing mice, Br. J. Haematol. 160 (2013) 766–778, https://doi.org/10.1111/bjh.12196.

[55] M. K, W. X, D. S, O. R, E. Ad, G. Bj, Adiponectin inhibits vascular endothelial growth factor-induced migration of human coronary artery endothelial cells, cardiovasc, Res. 78 (2008) 376–384, https://doi.org/10.1093/CVR.

[56] S.J. Prasanna, D. Gopalakrishnan, S.R. Shankar, A.B. Vasandan, Pro-inflammatory cytokines, IFNγ and TNFα, influence immune properties of human bone marrow and wharton jelly mesenchymal stem cells differentially, PloS One 5 (2010), e9016, https://doi.org/10.1371/journal.pone.0009016.

[57] L. Leroux, B. Descamps, N.F. Tojais, B. Séguy, P. Oses, C. Moreau, D. Daret, Z. Ivanovic, J.M. Boiron, J.M.D. Lamazière, P. Dufourcq, T. Couffinhal, C. Duplàa, Hypoxia preconditioned mesenchymal stem cells improve vascular and skeletal muscle fiber regeneration after ischemia through a wnt4-dependent pathway, Mol. Ther. 18 (2010) 1545–1552, https://doi.org/10.1038/mt.2010.108.

[58] A. Ray, Cytokines and their role in Health and disease: a brief overview, MOJ Immunol 4 (2016), https://doi.org/10.15406/moji.2016.04.00121.

[59] S.C. Heo, E.S. Jeon, I.H. Lee, H.S. Kim, M.B. Kim, J.H. Kim, Tumor necrosis factor-α-activated human adipose tissue-derived mesenchymal stem cells accelerate cutaneous wound healing through paracrine mechanisms, J. Invest. Dermatol. 131 (2011) 1559–1567, https://doi.org/10.1038/jid.2011.64.

[60] L. Zanotti, R. Angioni, B. Calì, C. Soldani, C. Ploia, F. Moalli, M. Gargesha, G. D'Amico, S. Elliman, G. Tedeschi, E. Maffioli, A. Negri, S. Zacchigna, A. Sarukhan, J.V. Stein, A. Viola, Mouse mesenchymal stem cells inhibit high endothelial cell activation and lymphocyte homing to lymph nodes by releasing TIMP-1, Leukemia 30 (2016) 1143–1154, https://doi.org/10.1038/leu.2016.33.

[61] D. Rodríguez, C.J. Morrison, C.M. Overall, Matrix metalloproteinases: what do they not do? New substrates and biological roles identified by murine models and proteomics, Biochim. Biophys. Acta Mol. Cell Res. 1803 (2010) 39–54, https://doi.org/10.1016/j.bbamcr.2009.09.015.

[62] R. Schäfer, G. Spohn, P.C. Baer, Mesenchymal stem/stromal cells in regenerative medicine: can preconditioning strategies improve therapeutic efficacy? Transfus. Med. Hemotherapy 43 (2016) 256–267, https://doi.org/10.1159/000447458.

[63] A.M. Bader, K. Klose, K. Bieback, D. Korinth, M. Schneider, M. Seifert, Y.-H. Choi, A. Kurtz, V. Falk, C. Stamm, Hypoxic preconditioning increases survival and pro-angiogenic capacity of human cord blood mesenchymal stromal cells in vitro, PloS One 10 (2015), e0138477, https://doi.org/10.1371/journal.pone.0138477.

[64] T. Kinoshita, K.W. Yip, T. Spence, F.F. Liu, MicroRNAs in extracellular vesicles: potential cancer biomarkers, J. Hum. Genet. 62 (2017) 67–74, https://doi.org/10.1038/jhg.2016.87.

[65] R.S. Lindoso, F. Collino, S. Bruno, D.S. Araujo, J.F. Sant'Anna, C. Tetta, P. Provero, P.J. Quesenberry, A. Vieyra, M. Einicker-Lamas, G. Camussi, Extracellular vesicles released from mesenchymal stromal cells modulate miRNA in renal tubular cells and inhibit ATP depletion injury, Stem Cell. Dev. 23 (2014) 1809–1819, https://doi.org/10.1089/scd.2013.0618.

[66] J. Zhang, S. Li, L. Li, M. Li, C. Guo, J. Yao, S. Mi, Exosome and exosomal microRNA: trafficking, sorting, and function, Dev. Reprod. Biol. 13 (2015) 17–24, https://doi.org/10.1016/j.gpb.2015.02.001.

[67] Y. Song, H. Dou, X. Li, X. Zhao, Y. Li, D. Liu, J. Ji, F. Liu, L. Ding, Y. Ni, Y. Hou, Exosomal miR-146a contributes to the enhanced therapeutic efficacy of interleukin-1β-primed mesenchymal stem cells against sepsis, Stem Cell. 35 (2017) 1208–1221, https://doi.org/10.1002/STEM.2564@10.1002/(ISSN)2157-6580.